https://doi.org/10.5194/egusphere-2026-2382
Preprint. Discussion started: 20 May 2026

Late Pleistocene Aggradation and Holocene Surface Reworking of Fluvial Terraces in the glacially overprinted Western Higher Himalaya

Jonas Kordt[1], Saptarshi Dey[2], Bodo Bookhagen[3], Georg Rugel[4], Johannes Lachner[4], Carlos Vivo-Vilches[4,5], Naveen Chauhan[6], Rasmus Thiede[1]

[1]Institute of Geosciences, Kiel University, Kiel, 24118, Germany
[2]Department of Geology and Geophysics, Indian Institute of Technology Kharagpur, 721302, India
[3]Institute of Geosciences, University of Potsdam, Potsdam, 14476, Germany
[4]Institute of Ion Beam Physics and Materials Research, Helmholtz-Zentrum Dresden-Rossendorf, Dresden, 01328, Germany
[5]Faculty of Physics, University of Vienna, Vienna, 1090, Austria
[6]Physical Research Laboratory, Ahmedabad, 380009, India

Correspondence to: Jonas Kordt (jonas.kordt@ifg.uni-kiel.de)

Abstract. Himalayan rivers are thought to undergo continuous adjustment in response to climatic variability, with changes in monsoon intensity and glacial extent playing a particularly important role in the Higher Himalaya. At the same time, short-term processes such as landslides, debris flows, and floods exert significant influence on both river dynamics and landscape morphology. We study a ~60 km long reach of the Ravi River in the western Higher Himalaya and a ~20 km reach of its main tributary, the Suil River, extending into the Sub-Himalaya. Using 12 new luminescence ages, 36 cosmogenic nuclide (^{10}Be and ^{26}Al) samples, remote sensing analysis, and detailed field observation, we reconstruct the formation of fluvial terraces and constrain the timing of subsequent erosion processes. We identify 10 recurring terrace levels, reaching elevations of up to ~225 m above the present rivers, with most terrace surfaces capped by a colluvial layer. The luminescence chronology documents repeated phases of fluvial aggradation, followed by major incision periods during the Late Pleistocene (~30 – 13 ky). In contrast, the cosmogenic surface exposure ages do not reveal terrace abandonment ages, but indicate distinct, Late-to-Mid Holocene reworking (~7 – 2 ky) on all but two terrace surfaces. Our topographic analysis suggests that up to ~50% of the Ravi and Suil catchment areas may have been influenced by glacial coverage during the Late Pleistocene, likely contributing significantly to sediment aggradation during this time. The Holocene surface exposure ages, in contrast, are interpreted to reflect post-depositional modification by mass wasting processes (e.g., landslides or debris flow) and, in some cases, by potentially vigorous glacial lake outburst floods.

1 Introduction

Rivers along the rapidly uplifting Himalayan Mountain front are subject to continuous adjustment. Numerous studies have shown that active tectonics can induce river blockages and differential uplift, leading to the formation of knickpoints and persistent modification of longitudinal river profiles (e.g., Seeber and Gornitz, 1983; Ouchi, 1985; Kirby and Whipple,

https://doi.org/10.5194/egusphere-2026-2382
Preprint. Discussion started: 20 May 2026

2001). At the same time, climatic variability drives a range of processes - such as fluctuations in monsoon intensity and glacial extent - that strongly influence runoff, erosion, and stream power across annual to multimillennial timescales (e.g., Bookhagen et al., 2006; Dosseto et al., 2018; Dey et al., 2023). These changes affect both the hydrologic and sediment budgets of river systems, ultimately controlling fluvial regimes and determining whether rivers operate under transport- or supply-limited conditions. In transport-limited settings, insufficient transport capacity relative to sediment load leads to aggradation, whereas in supply-limited systems, excess transport capacity promotes channel incision (e.g., Montgomery and Buffington, 1997; Simon and Rinaldi, 2006; Julien, 2012). However, the relative importance of these mechanisms and their geomorphic consequences remain the subject of ongoing debate (e.g., Ray and Srivastava, 2010; Scherler et al., 2015; Dey et al., 2022; Tofelde et al., 2022; Chauhan et al., 2026). One key mechanism involves the coupling between climate variability, glacier dynamics, and river response. This relationship is inherently complex, as different feedbacks within the system can act in opposing directions. For example, an increase in monsoon intensity generally enhances transport capacity, but it can also increase erosion rates and sediment supply (e.g., Pratt et al., 2002; Clift et al., 2008; Dey et al., 2022). Moreover, stronger monsoon conditions may promote glacier growth, provided that temperatures at high elevations remain sufficiently low (e.g., Benn and Owen, 1998; Bolch et al., 2012; Owen and Dortch, 2014). River response is further modulated by position along the longitudinal profile, with upstream and downstream reaches potentially reacting differently to the same external forcing (e.g., Schumm, 1977; Ray and Srivastava, 2010; Densmore et al., 2016). It is crucial to understand the past responses of Himalayan river systems to external factors in different locations, especially in Himalayan river basins with repeated high glacial coverage during the Late Quaternary (e.g., Barnard et al., 2004; Ray and Srivastava, 2010; Eugster et al., 2016; Dey et al., 2023).

In addition to long-term trends of aggradation and incision, Himalayan river systems are strongly influenced by short-term mass wasting processes. In the steep valleys of the Greater Himalaya in particular, populations are exposed to natural hazards such as landslides, debris flows, and floods, the frequency and magnitude of which are modulated by both climatic variability and tectonic activity (e.g., Shroder and Bishop, 1998; Bookhagen et al., 2005; Dortch et al., 2009; Dimri et al., 2016; Dubey et al., 2023). Extreme flood events may also be triggered by glacial lake outburst floods (GLOFs) or the sudden failure of landslide-dammed lakes (e.g., Ruiz-Villanueva et al., 2017; Andermann et al., 2023; Veh et al., 2020). Such high-magnitude events can rapidly alter local base levels by several tens of meters and initiate cascades of secondary erosional processes upstream of the flood zone (Cook et al., 2018; Chen et al., 2025; Sattar et al., 2025). In recent decades, these events have caused severe damage to infrastructure and resulted in significant loss of life (e.g., Watanbe and Rothacher, 1996; Allen et al., 2016; Ruiz-Villanueva et al., 2017). A better understanding of the timing and frequency of such events in the past is therefore essential for identifying their driving mechanisms, including the roles of climatic change and glacial retreat.

In this study, we investigate long-term Late Pleistocene aggradation and incision patterns preserved in fluvial terrace sequences, as well as the imprint of short-term mass wasting events and flood-related processes along two Himalayan rivers. The Ravi and Suil Rivers are located in the western Himalaya, originating in the Pir Panjal Range before converging at the

https://doi.org/10.5194/egusphere-2026-2382
Preprint. Discussion started: 20 May 2026

Chamera reservoir and exiting the Greater Himalaya as the Ravi River (Fig. 1), eventually joining the Indus River system. The study area is strongly influenced by climatic gradients: the Pir Panjal Range exhibits extensive glaciation, while the adjacent Dhauladhar Range to the south is subject to intense monsoonal precipitation (GLIMS and NSIDC, 2005 [updated 2018]; Funk et al., 2014). As a result, both river systems are sensitive to variations in monsoon intensity and fluctuations in glacial extent, particularly during the Pleistocene. We examine fluvial terraces along an approximately 60 km reach extending from the Higher Himalaya north of the Dhauladhar Range to the transition into the Siwalik foreland within the Sub-Himalaya (Fig. 1). An initial optically stimulated luminescence (OSL) chronology for this river basin was established by Joshi et al. (2022); here, we expand upon this framework by incorporating new OSL ages to refine the Late Quaternary depositional history of the Ravi and Suil catchments. To assess the influence of climatic forcing, we compare reconstructed aggradation–incision cycles with published records from river systems along the southern Himalayan front (Srivastava et al., 2009; Thakur et al., 2014; Dey et al., 2016b; Kapannusch et al., 2020; Dey et al., 2022; Chauhan et al., 2026). In addition, we apply cosmogenic nuclide (^{10}Be and ^{26}Al) dating to terrace surfaces, which reveals widespread Holocene surface reworking. Most terraces are mantled by colluvial deposits, indicating substantial post-depositional modification. Based on these observations, we reconstruct the timing of Holocene surface activity and evaluate potential driving processes, including mass wasting and flood events such as GLOFs. The combined dataset allows us to assess possible triggers, including variations in monsoon strength and glacial retreat. Together, our new field observations and geochronological data, in combination with previous results from Joshi et al. (2022), provide improved insight into the interplay of climate forcing, sediment dynamics, and mass wasting processes along the western Greater Himalayan front.

https://doi.org/10.5194/egusphere-2026-2382
Preprint. Discussion started: 20 May 2026

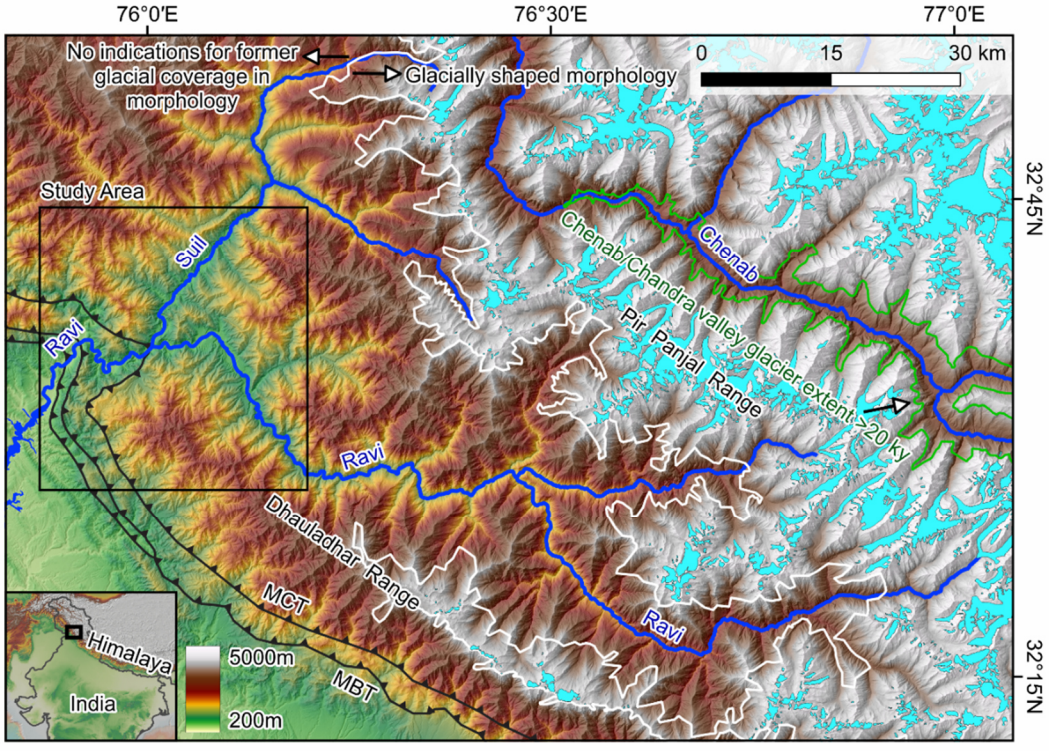

Figure 1: Topographic map of the study area and the Ravi and Suil headwaters showing present glacial coverage (light blue coloured areas) and potential past glacial morphology (white outlined areas). The boundary between glacially and non-glacially shaped morphology was mapped by using multiple terrain attributes (topography, roughness, relief), satellite imagery, field observations in the Ravi Region, and findings of traverses through the area conducted while sampling rocks used for thermochronologic dating (Deeken et al., 2011). It should be noted that this does not indicate continuous glacial coverage across the entire area, as numerous valleys, especially along steep upper mountain flanks, lack evidence for former glaciation. Please note that large sections of the Ravi headwaters have a glacially shaped morphology and contain presently active glaciers in the Pir Panjal Range and the northern side of the Dhauladhar Range. The extent and reconstruction of the more than 1 km thick main Chenab/Chandra valley glacier prior to 20 ky is adopted from the previous study by Eugster et al. (2016) and documents the extended past glacial coverage of the region. Tectonic boundaries after Steck (2003), present-day glaciers data by GLIMS and NSIDC (2005 [updated 2018]), and DEM taken from JAXA (AW3D30).

2 Geological Setting

The Ravi River is a moderately sized river in the northwestern Himalaya, with a ~5560 km² catchment within the Higher Himalaya. It is a tributary to the Chenab and Indus River systems. The Ravi originates in the Chamba region and is mainly sourced from glaciers of the Pir Panjal range. After an initial flow direction toward the southwest, it turns northwest and flows within a steep valley parallel to the northern flank of the Dhauladhar Range. Around Chamba, the Ravi River valley gets less steep, and fluvial aggradational terraces develop. Approximately 10 km north of Dalhousie, the Ravi River is joined by its tributary, the Suil River, which originates from glaciers in the Pir Panjal Range about 50 km further north. This confluence occurs just upstream of the Chamera Dam, where an artificial reservoir was created by damming the Ravi River

https://doi.org/10.5194/egusphere-2026-2382
Preprint. Discussion started: 20 May 2026

in the 1990s. Downstream of the confluence, the Ravi exits the Higher Himalayan Mountain front and enters the Sub-Himalayan belt.

Our study area comprises an approximately 60 km long reach of the Ravi River and a ~20 km section of the Suil River, spanning areas upstream and downstream of their confluence (Fig. 1). The lower valley reaches are characterized by a well-developed sequence of strath and fill terraces, reaching elevations of up to ~225 m above the present river channels. Such extensive terrace preservation contrasts with the strongly glacially overprinted headwater regions, where these features are comparatively rare. In addition, the studied river sections are, on average, less steep than their upstream counterparts (Supplement Fig. S1) and display broader, more open valley geometries with relatively wide valley floors, frequently interrupted by terrace levels. This changing geometry mostly aligns with the varying height and uplift of the Dhauladhar Range. In the central section of the range with high peaks above 5 km, previous studies have identified high uplift rates since the Middle Miocene (Deeken et al., 2011; Thiede et al., 2017). This uplift has been attributed to the Main Boundary thrust (MBT) (Deeken et al., 2011; Thiede et al., 2017), which, together with the nearby Main Central Thrust (MCT), sits in the footwall of the Dhauladhar Range. The central range is likely part of a proposed MBT ramp, which may extend north up to the Ravi (Thiede et al., 2017), resulting in a steep river valley. In contrast, the Dhauladhar Range elevation dips to below 3 km and features lower exhumation rates in the northwest (Deeken et al., 2011; Adlakha et al., 2013), potentially leading to a wider valley. A previous study identified 8 terrace levels in this section (Joshi et al., 2022), and we recognized 10 recurring levels, although some are just fluvial incision cuts into higher fill-terrace levels.

The main geologic unit exposed in the Ravi and the Suil Rivers is the Higher Himalayan metasediment (Fig. 2). In the study area, this exposed material is also known as the Chamba or Haimata formation and consists of a large variety of low to medium-grade metamorphic sediments, including slate, schist, quartzite, and metagreywacke (Fuchs, 1975; Thakur, 1998; Chambers et al., 2009). The Suil River crosses a small exposed section of the Tethyan Sequence folded into a syncline, which comprises sediments and low-grade metamorphic rocks (Fuchs, 1975; Thakur, 1998; Sharma and Bhola, 2005). For the Ravi River, the Dhauladhar Range is also an important source of material, consisting mostly of the Higher Himalayan Crystalline Granites and Gneiss intrusions of Cambrian and Ordovician age (Jaegaer, 1971; Le Fort, 1975; Bhanot et al., 1974; Dhiman and Singh, 2019). Downstream of the Chamera Dam, which is in the vicinity of the MCT, the Ravi enters the Lesser Himalayan Sequence, which consists mostly of sediments, volcanics, and low- to medium-grade metasediments (Gansser, 1981; Thakur, 1992). Near the village Kairi, at the MBT, the Ravi enters the Sub-Himalaya (Fig. 2), where the low-grade metamorphic sedimentary Dharamshala Sequence alternates with the Lower-, Middle-, and Upper-Siwalik sediments (Brozovic and Burbank, 2000; White et al., 2002; Najman et al., 2004).

https://doi.org/10.5194/egusphere-2026-2382
Preprint. Discussion started: 20 May 2026

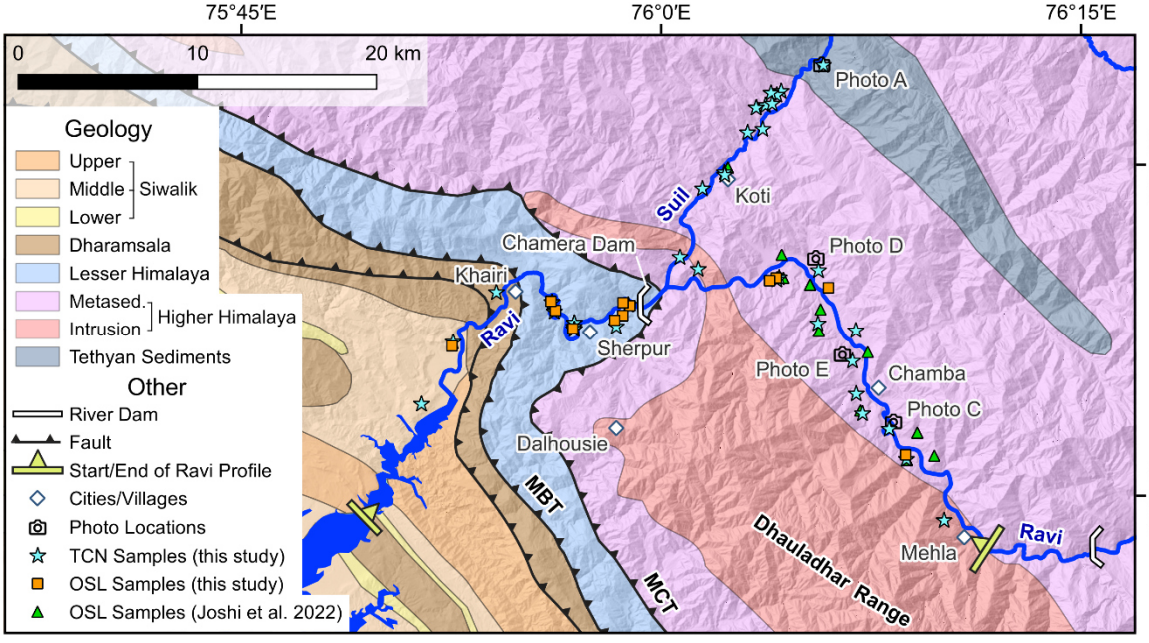

Figure 2: Geological map with hillshade of the Ravi and Suil River study area, including all sample locations. The start and end of the Ravi Profile (yellow) in Fig. 8 are shown. Photo locations correspond to pictures in Fig. 6. Abbreviations: OSL = Optically Stimulated Luminescence, TCN = Terrestrial Cosmogenic Nuclide, Metased. = Metasediment. Lithological and tectonic boundaries after Steck (2003) and Gavillot et al. (2018). DEM by JAXA (AW3D30).

3 Methodology and Data

3.1 Cosmogenic nuclide dating

Cosmogenic nuclide dating using terrestrial ^{10}Be and ^{26}Al concentrations in quartz has been successfully used in the past in this area to constrain surface-exposure ages of alluvial fans and fluvial terraces (e.g., Bookhagen et al., 2006; Dey et al., 2016b). To determine the exposure ages of the terraces, we collected 36 samples from the Ravi and Suil Rivers (cf. Table 1 and Fig. 2 for location). All samples represent amalgamations of 20 – 25 small pebbles with diameters of 2 – 3 cm and were collected within the upper 5 – 6 cm of the surface (Anderson et al., 1996).

Samples were crushed and sieved to retrieve the 250 – 500 µm fraction, which had been further processed for magnetic, heavy-liquid separation, and initial cleaning with diluted HCl. Further cleaning with H_2SiF_6 was performed following Brown et al. (1991) to obtain clean quartz, and additional leaching with 1 – 2% HF was carried out according to standard laboratory protocols by Kohl and Nishiizumi (1992). The quartz grains were dissolved in HF, and ~90 µl of 3.2×10^{-3} g/g ^{9}Be carrier in 1N HCl with density 1.010 g/cm^3 (the in-house carrier at the University of Potsdam, derived from Beryllium-bearing Phenakite from a mine in Brazil) was added. No ^{27}Al carrier has been added, except for blanks, which contained 2 mg Al. Ion-exchange column chemistry to extract Be and Al was performed at the University of Potsdam following Blanckenburg

https://doi.org/10.5194/egusphere-2026-2382
Preprint. Discussion started: 20 May 2026

(2005). Extracted $Be(OH)_2$ and $Al(OH)_3$ were oxidised, and Nb (Be) and Ag (Al) powder were added in mixing ratios of ~4:1 for Nb:Be and ~1:1 for Ag:Al. Radionuclide measurements were conducted at the Accelerator Mass Spectrometer DREAMS in Helmholtz-Zentrum Dresden-Rossendorf (Rugel et al., 2016; Lachner et al., 2023). The calibration of the ^{10}Be measurement was done using an in-house reference material "SMD-Be-12" ($^{10}Be/^{9}Be$ = (1.704 ±0.030) $\times10^{-12}$), which is traceable to the primary standard material NIST4325, and the calibration of ^{26}Al was done using "SMD-Al-11" ($^{26}Al/^{27}Al$ = (9.66 ±0.14) $\times10^{-12}$), which is traceable to the primary standard MB04 (Akhmadaliev et al., 2013). The averaged procedure blank values (n=6) were measured together with the samples and propagated through all calculations. The average values for the first sample run (all NWR and SD samples) are 2.25±0.63 $\times10^{-15}$ for $^{10}Be/^{9}Be$ and 6.31±2.25 $\times10^{-15}$ for $^{26}Al/^{27}Al$, while the values for the second sample run (all JK samples) are 3.19±0.55 $\times10^{-15}$ for $^{10}Be/^{9}Be$ and 8.43±7.50 $\times10^{-15}$ for $^{26}Al/^{27}Al$. After converting the sample ratios to ^{10}Be and ^{26}Al concentrations, we used the time-dependent spallogenic production scheme by Lifton et al. (2014) in the CRONUS-Earth online calculator version 3 (Balco et al., 2008) to calculate the surface exposure ages. We used measurements of the erosion rate from the existing literature for similar settings (Phillips et al., 2006; Ritz et al., 2006; Stübner et al., 2021) that show a range of 1 – 12 mm/ky. We rely on a low erosion rate of 5 mm/ky for our calculations. Results with 0 mm/ky only differ very slightly (below 5% for all samples, see Supplement Table S1). Higher erosion rates are going to result in older surface exposure ages, but for most of our samples, the difference is small, because the samples have Holocene ages. For example, calculations with a nearly one-order of magnitude higher erosion rate of 40 mm/ky show that only the three oldest samples have a deviation of more than 25%, but still below 50% (Supplement Table S1). We also verified the influence of an inheritance signal and processed two additional samples from at least 10 m depth within two terraces. Their average concentrations (4.65 $\times10^{3}$ atoms g^{-1} for ^{10}Be and 3.53 $\times10^{4}$ atoms g^{-1} for ^{26}Al) both result in an apparent age of 1.0 ky. This is more than 25% of the youngest 12 ages, but less for the remaining 24 samples. However, as we do not have an inheritance for all terrace levels, we decided against subtracting the measured inheritance from all values, which might result in some samples appearing too old. Although the $^{26}Al/^{10}Be$ ratios of our inheritance samples equal 6.75 including uncertainty, six of our surface samples have $^{26}Al/^{10}Be$ ratios below 6.75 with uncertainty, indicating a potential burial signal that could raise sample inheritance (Granger, 2006; Bhattacharjee et al., 2023). We discuss the impact of all the mentioned potential errors on our results in Discussion 5.1.

Sample Name	Location	Sample Height (m asl)	Topographic Shielding	Sample Weight (g)	^{10}Be (10^3 atoms g^{-1})	^{10}Be Uncertainty (10^3 atoms g^{-1})	^{26}Al (10^3 atoms g^{-1})	^{26}Al Uncertainty (10^3 atoms g^{-1})	$^{26}Al/^{10}Be$	$^{26}Al/^{10}Be$ Uncertainty	^{10}Be Age (ky)	^{26}Al Age (ky)
NWR21-41	76.056° E 32.697° N	972	0.99	29.37	27.3	1.5	235	26	8.6	1.1	4.9 ± 0.4	6.1 ± 0.9
NWR21-43	76.066° E 32.699° N	801	0.96	29.42	12.0	1.3	86	10	7.2	1.2	2.6 ± 0.3	2.6 ± 0.4
NWR21-46	76.037° E 32.664° N	846	0.96	30.09	28.1	2.2	210	16	7.5	0.8	5.7 ± 0.6	6.1 ± 0.7
NWR21-48	75.935° E 32.596° N	689	0.97	30.12	23.5	1.9	158	24	6.7	1.2	5.4 ± 0.6	5.2 ± 0.9
NWR21-50	75.875° E 32.581° N	662	0.99	29.84	33.2	2.2	262	37	7.9	1.2	7.4 ± 0.7	8.4 ± 1.5
NWR21-52	75.947° E 32.588° N	669	0.98	22.69	12.0	1.1	74	12	6.2	1.2	2.8 ± 0.3	2.4 ± 0.5
NWR21-53	75.947° E 32.590° N	719	0.98	12.77	27.5	2.4	200	18	7.3	0.9	6.1 ± 0.7	6.4 ± 0.8
SD17CRN02	76.143° E 32.520° N	1113	0.98	16.14	108.8	6.7	557	34	5.1	0.4	16.5 ± 1.5	12.5 ± 1.4

https://doi.org/10.5194/egusphere-2026-2382
Preprint. Discussion started: 20 May 2026

SD17CRN12	76.067° E 32.611° N	873	0.99	13.72	29.6	2.4	204	16	6.9	0.7	5.7 ± 0.6	5.7 ± 0.7
SD17CRN14	75.947° E 32.587° N	665	0.98	6.49	8.1	2.8	59	34	7.2	4.8	1.8 ± 0.6	1.8 ± 1.1
SD17CRN16	75.901° E 32.606° N	688	0.99	7.28	8.2	2.7	54	32	6.6	4.4	1.8 ± 0.6	1.6 ± 1.0
SD17CRN17	75.855° E 32.550° N	669	1.00	9.69	10.9	2.1					2.4 ± 0.5	
JK-22-09	76.069° E 32.612° N	871	0.99	49.40	16.4	2.4	77	37	4.7	2.3	3.1 ± 0.5	2.0 ± 1.0
JK-22-12	76.010° E 32.623° N	795	0.97	43.29	34.8	3.4	188	36	5.4	1.2	7.2 ± 0.9	5.6 ± 1.2
JK-22-14	76.051° E 32.685° N	890	0.99	50.50	30.8	2.8					5.9 ± 0.7	
JK-22-15	76.071° E 32.706° N	943	0.98	41.46	17.7	3.5	3180	318	179.9	183.5	3.2 ± 0.7	
JK-22-16	76.068° E 32.704° N	933	0.97	50.17	21.8	2.1					4.1 ± 0.5	
JK-22-17	76.065° E 32.705° N	983	0.99	44.98	21.6	6.8	140	20	6.5	2.3	3.8 ± 1.3	3.5 ± 0.6
JK-22-20	76.062° E 32.699° N	930	0.99	34.89	18.3	3.3	161	41	8.8	2.8	3.3 ± 0.6	4.2 ± 1.2
JK-22-21	76.056° E 32.697° N	971	0.99	45.33	36.7	3.5	258	98	7.0	2.7	6.6 ± 0.8	6.7 ± 2.7
JK-22-23	76.096° E 32.718° N	1043	0.98	34.52	33.3	2.6	287	25	8.6	1.0	5.7 ± 0.6	7.0 ± 0.9
JK-22-24	76.060° E 32.687° N	835	0.98	43.29	18.9	1.9	82	18	4.4	1.1	3.8 ± 0.4	2.3 ± 0.6
JK-22-25	76.037° E 32.665° N	836	0.95	37.71	23.5	2.0	196	88	8.3	3.8	4.9 ± 0.5	5.8 ± 2.7
JK-22-26	76.021° E 32.617° N	934	0.99	39.93	23.3	1.6	104	30	4.5	1.3	4.3 ± 0.4	2.8 ± 0.8
JK-22-27	76.092° E 32.615° N	812	0.96	36.48	10.1	1.2	116	120	11.4	11.9	2.0 ± 0.3	
JK-22-28	76.114° E 32.585° N	864	0.98	29.67	12.2	1.1	80	25	6.6	2.1	2.4 ± 0.3	2.2 ± 0.7
JK-22-33	76.133° E 32.535° N	911	0.97	46.15	33.0	1.8					6.4 ± 0.5	
JK-22-36	76.165° E 32.489° N	1413	0.96	23.28	81.4	5.2	484	63	5.9	0.9	10.8 ± 1.0	9.4 ± 1.5
JK-22-40	76.117° E 32.543° N	1035	0.98	32.89	29.6	1.6	181	68	6.1	2.3	5.2 ± 0.4	4.5 ± 1.8
JK-22-42	76.114° E 32.553° N	985	0.99	48.15	34.5	1.3	163	18	4.7	0.5	6.2 ± 0.4	4.2 ± 0.6
JK-22-43	76.112° E 32.569° N	963	0.99	48.19	25.0	1.2	173	42	6.9	1.7	4.5 ± 0.3	4.5 ± 1.2
JK-22-46	76.092° E 32.588° N	940	0.99	40.75	22.4	1.3					4.1 ± 0.3	
JK-22-48	75.947° E 32.590° N	719	0.98	48.65	20.1	1.1	147	48	7.3	2.4	4.4 ± 0.4	4.6 ± 1.6
JK-22-49	75.947° E 32.587° N	669	0.98	47.65	23.0	1.1	131	14	5.7	0.7	5.3 ± 0.4	4.3 ± 0.6
JK-22-51	75.934° E 32.601° N	656	0.97	34.62	19.8	1.3	369	373	18.6	18.9	4.6 ± 0.4	
JK-22-59	75.972° E 32.588° N	981	0.99	16.00	32.5	2.5	283	135	8.7	4.2	5.8 ± 0.6	7.2 ± 3.6

Table 1: Cosmogenic nuclide sample information, including concentrations and calculated ages. For details about the calculation, see Section 3.1. ^{26}Al results with an underscore have a low measurement output, which we consider unreliable. All ages are calculated with an erosion rate of 5 mm/ky. For results with other erosion rates, see Supplement Table S1.

3.2 Optically stimulated luminescence (OSL) dating

OSL dating is widely used for constraining the sediment burial time across diverse sedimentary environments (e.g., Singhvi et al., 2022 and references therein). Despite having a tendency for weak luminescence sensitivity (Parida et al., 2025) and heterogeneous bleaching due to rapid transport, many studies have successfully applied OSL dating of Himalayan quartz (e.g., Thakur et al., 2014; Dey et al., 2022). In this study, we collected a total of 12 fine-to-medium sand samples in 22 cm-

https://doi.org/10.5194/egusphere-2026-2382
Preprint. Discussion started: 20 May 2026

long light-sealed metal tubes. All samples have been collected from terraces along the Ravi River (Fig. 2). We collected 9 samples within the upper 5 meters of the terraces ("Near top") and 3 samples within the lower 7 meters of the terraces ("Near bottom").

The 'clean' quartz was extracted from the samples in darkroom laboratory conditions following the protocol by Aitken (1998). Radiation measurements were done with a Risoe automated OSL-TL reader DA-20 at the Physical Research Laboratory Ahmedabad. It is equipped with a Blue LED source and a Hoya U-340 filter fitted before the photomultiplier tube for detection (Lapp et al., 2015). Quartz purity was checked using IR test, where IR stimulation for 60s was used at 50°C to detect feldspar. Due to 10 – 30% of feldspar contamination (even after 2x treatment with 40% HF), we chose the Double SAR (Single Aliquot Regenerative) protocol for equivalent dose (De) estimation (Roberts, 2007). The additional step of IR wash for 60s before using the usually-practised SAR (Murray and Wintle, 2003) effectively eradicates the feldspar contribution to OSL measurement. 24 aliquots of each sample were measured with regenerative doses set between 40 Gy and 180 Gy, test dose was 10 Gy, and the preheat temperature was 240°C. The aliquots were considered for equivalent Dose (De) estimation only if (i) the recycling ratio was within 1±0.1; (ii) the ED error was less than 20%; (iii) test dose error was less than 10%; and (iv) recuperation was below 5% of the natural. Residual doses were checked with present-day Ravi River sand that has the same grain size as the terrace samples (2 samples) (Hu et al., 2010). The over-dispersion values are less than 30%; hence, the Central Age Model has been used for the estimation of De (Bailey and Arnold, 2006). The moisture content of individual samples was measured by subtracting the dry from saturated sample weight. U, Th, and K content for individual samples were measured in a high-purity Germanium detector and were further used to calculate the corresponding dose rates following Durcan et al. (2015). Information about OSL-IRSL ages is listed in Table 2.

Sample Name	Location	Type of sample	Height (m asl)	U (ppm)	Th (ppm)	K (%)	H_2O (%)	Paleodose (Gy)	Dose Rate (Gy/ky)	Central Age (ky)
SD-R-01	76.143° E 32.522° N	Near Top	1021	3.3 ± 0.2	22.4 ± 1.3	2.29 ± 0.11	20 ± 2	108 ± 10.6	3.86 ± 0.10	28.0 ± 2.9
SD-R-02	76.067° E 32.612° N	Near Top	869	3.3 ± 0.2	18.7 ± 0.9	2.61 ± 0.13	14 ± 2	122 ± 10	4.08 ± 0.11	29.5 ± 2.6
R-OSL-04	75.946° E 32.587° N	Near Top	677	3.4 ± 0.2	18.0 ± 0.9	2.17 ± 0.12	20 ± 2	69 ± 4.6	3.89 ± 0.10	17.7 ± 1.3
R-OSL-05	75.936° E 32.596° N	Near Top	712	3.5 ± 0.2	16.9 ± 0.8	1.97 ± 0.10	19 ± 2	73.4 ± 6.1	3.57 ± 0.10	20.5 ± 1.8
R-OSL-06	75.933° E 32.601° N	Near Top	651	3.3 ± 0.2	12.2 ± 0.6	1.99 ± 0.1	18 ± 2	43.4 ± 2.3	3.16 ± 0.10	13.4 ± 0.9
SD-18-02	75.874° E 32.579° N	Near Top	658	3.1 ± 0.1	22.7 ± 0.8	2.34 ± 0.17	13 ± 2	119.4 ± 8.3	4.09 ± 0.16	27.7 ± 2.2
SD-18-04	76.098° E 32.607° N	Near Top	849	3.0 ± 0.2	15.9 ± 0.7	1.95 ± 0.1	18 ± 2	43.2 ± 2.3	3.26 ± 0.09	13.2 ± 0.8
SD-R1	75.980° E 32.599° N	Near Bottom	751	3.0 ± 0.2	19.4 ± 0.6	2.11 ± 0.1	20 ± 2	63.5 ± 2.8	3.48 ± 0.10	18.3 ± 0.9
SD-R5	75.976° E 32.594° N	Near Top	1000	2.8 ± 0.2	16.9 ± 0.6	1.98 ± 0.1	17 ± 2	42.6 ± 2.4	3.41 ± 0.12	12.5 ± 0.8
SD-R2	75.976° E 32.600° N	Near Bottom	746	3.4 ± 0.1	23.5 ± 0.7	2.5 ± 0.1	18 ± 2	79.1 ± 5.4	4.26 ± 0.11	18.6 ± 1.3
SD-R3	75.971° E 32.591° N	Near Top	949	2.8 ± 0.1	18.1 ± 0.7	1.91 ± 0.1	20 ± 2	44.6 ± 2.5	3.27 ± 0.12	12.9 ± 0.9
SD-18-05	76.063° E 32.610° N	Near Bottom	763	3.0 ± 0.2	18.9 ± 0.8	2.77 ± 0.1	16 ± 2	70 ± 6.4	4.19 ± 0.13	16.7 ± 1.6

Table 2: OSL sample data and corresponding radioactive material concentrations, environmental dose rates, and calculated ages.

https://doi.org/10.5194/egusphere-2026-2382
Preprint. Discussion started: 20 May 2026

4 Results

4.1 Terrace levels and sediment characteristics

Throughout the studied Ravi and Suil River sections, we identified 10 terrace levels (see Fig. 3 for mapped terraces and Fig. 4 for example of raw relative elevation data). The first level (T1) up to 5 m above the current day rivers, is still active during higher water levels and thus no permanent vegetation is present. The next higher terrace level T2 is at ~10 – 20 m above the rivers. Both T1 and T2 are commonly found along the Ravi and Suil Rivers and often represent fans of local tributaries. The next three levels are T3 at ~25 m above the river, T4 at ~40 m height, and T5, which is only present at the Ravi, at ~50 – 55 m above the river. These three levels are less abundant than the lowest ones. In some places (e.g., ~2 km south of Chamba) we observe that these levels are just cut down from the higher T6 or T7 terrace fill material, which is confirmed by one OSL age. We did not find any evidence that these three levels have been deposited independently from other levels by the Ravi or Suil Rivers. Above these three levels is level T6, which is widespread and forms larger terraces at ~60 – 85 m height along the Ravi and Suil River sections. The next higher level (T7) is less common in both catchments at ~96 – 110 m above the present river level. In the Suil River catchment, we identified a higher terrace level (T8) at 120 – 125 m height that is present north of the village Koti. However, it appears that this level is just cut down from the T9 terrace fill material above, although we could not always verify that due to limited access. Level T9, around ~130 – 167 m above the present Ravi and Suil Rivers, is well preserved and frequently exposed along the investigated river sections. The highest level T10 has a height of ~200 – 225 m and is less abundant than T9. Above this highest level, we find remnants of two isolated higher terraces: one at ~300 – 350 m above the Ravi, just a few hundred meters downstream of the Chamera dam after the confluence of the Ravi and Suil Rivers (Fig. 3D). The second terrace is at ~430 m height above the Ravi, ~1.5 km north of the village Mehla (Fig. 3A). However, as both terraces do not contain much fluvial material and are not abundant elsewhere, we do not include them in our terrace sequence. The widespread levels are also visible in our combined histogram and kernel density estimate plots (Fig. 5) that show the height distribution of flat surfaces around the Ravi and Suil River sections. Our photo of the mapped terraces near Chamba also shows the widespread terrace occurrence (Fig. 6E).

https://doi.org/10.5194/egusphere-2026-2382
Preprint. Discussion started: 20 May 2026

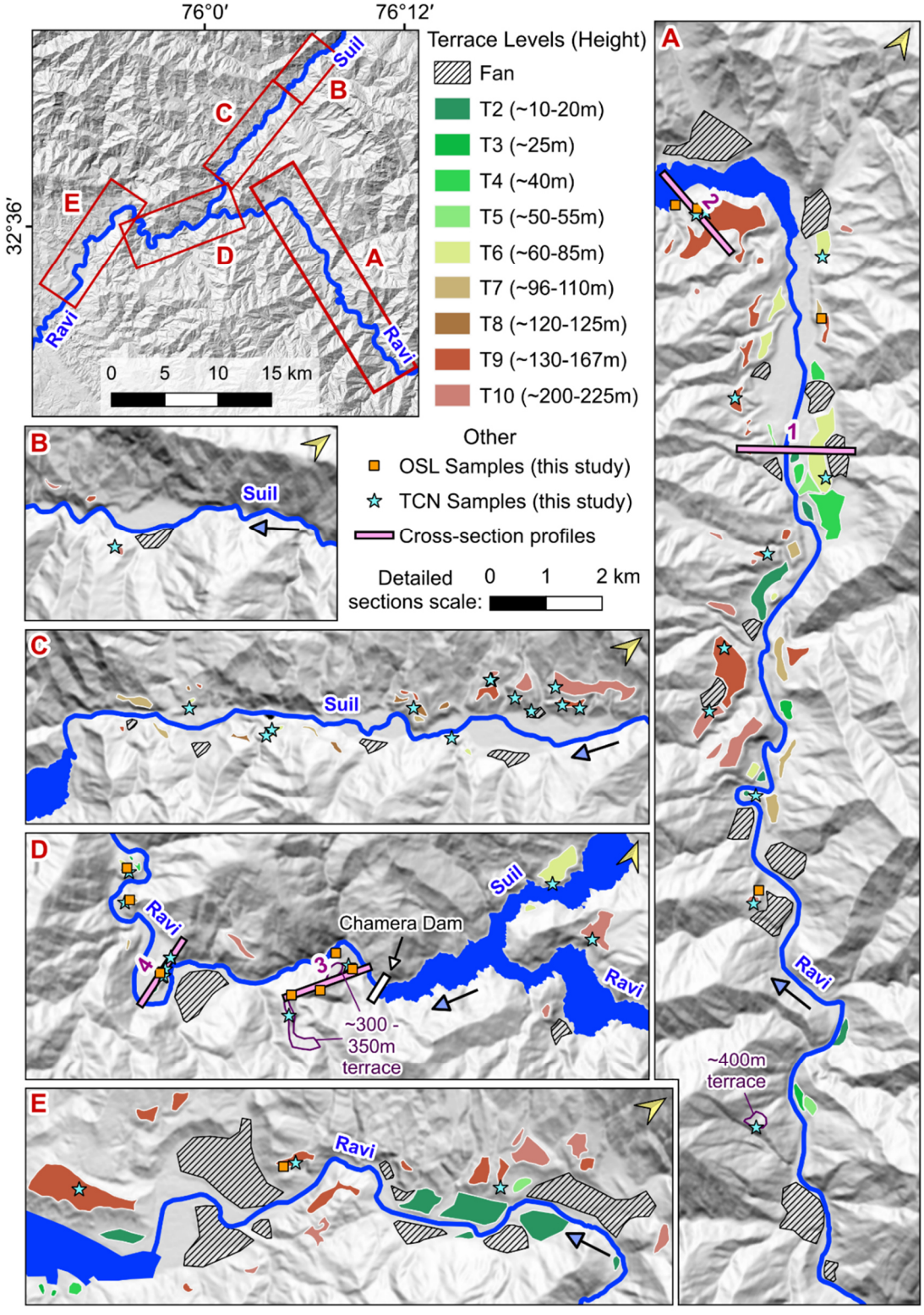

https://doi.org/10.5194/egusphere-2026-2382
Preprint. Discussion started: 20 May 2026

Figure 3: Terrace map of the studied Ravi and Suil River sections with a hillshade as background map, including sample locations, tributary fans, and cross-section profiles shown in Fig. 7. The top left map corresponds to the "study area" rectangle in Fig. 1 and shows an overview of all detailed sections (A-E). Arrows alongside rivers indicate flow direction. We only manually mapped terraces of at least 10 meter height above the present rivers, a minimum size of 8000 m², and maximum slope of 5° at the terrace centre. DEM by JAXA (AW3D30).

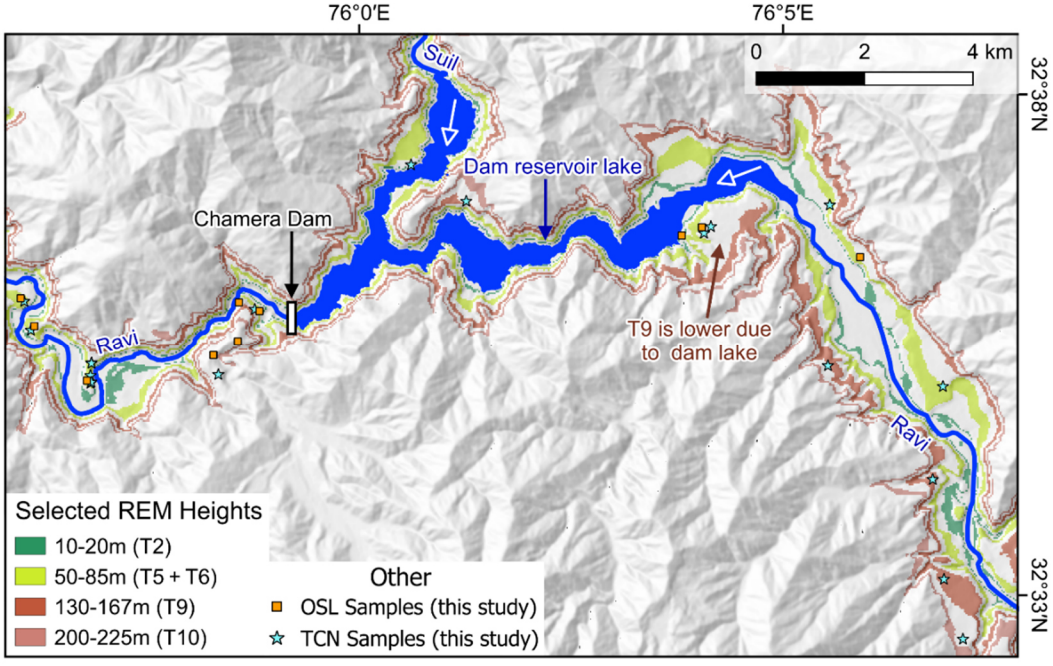

Figure 4: Relative Elevation Model (REM) of the Suil and Ravi Rivers confluence region. Only selected heights of the most prominent terraces are shown. Sample locations of luminescence and cosmogenic nuclide samples are included. White arrows within rivers indicate flow direction. Please note that due to the reservoir lake, the terrace REM height next to it is lower than before the dam construction. DEM by JAXA (AW3D30).

https://doi.org/10.5194/egusphere-2026-2382
Preprint. Discussion started: 20 May 2026

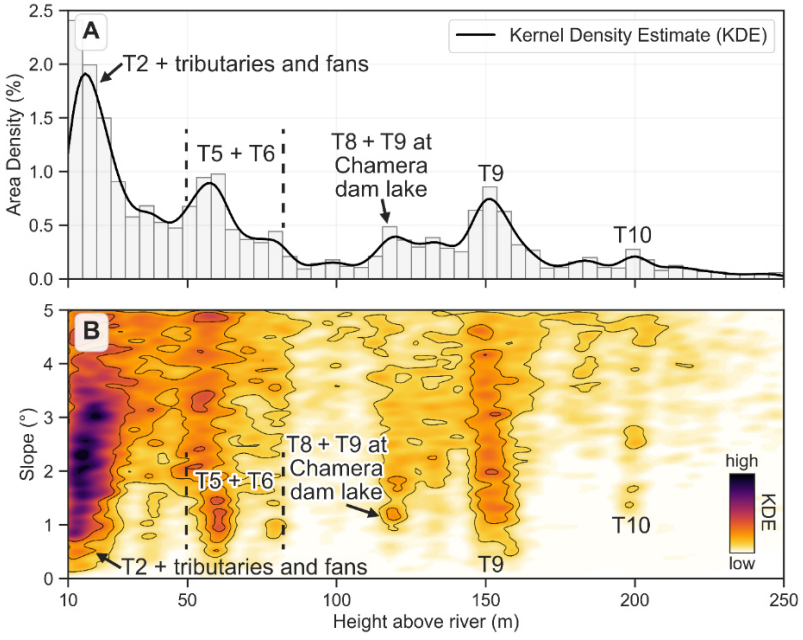

Figure 5: Combined river-height histogram and 2D river-height and slope Kernel Density Estimate (KDE) plot showing the widespread terrace levels along the studied Ravi and Suil River sections (cf. Fig. 3). For both plots, we only use the digital elevation model heights (Resolution: 30 m) from 10 to 250 meters where the slope is ≤ 5°. **A**: Histogram of the filtered height values shows their distribution as area density in percent. For the smoothing KDE curve, we used a bandwidth of 0.2. **B**: 2D-KDE plot based on the same filtered height values, but now including the corresponding slope values using a bandwidth of 0.4. Darker colours show a higher density estimation of the area. Please note that tributary fans and their riverbeds lead to an overestimation of the lower terrace levels up to ~60 m, especially for T2. Below the T9 level (120-140 m) are some terrace surfaces shown with heights that are impacted by the sedimentation related to the Chamera dam. These heights are lower than T9, although this is the same terrace level. We also show the height distribution using the mapped terraces only in Supplement Fig. S2.

Most terraces preserved along the Ravi and Suil Rivers show a dip of ~2 – 5° towards the river. This contributes to the scattering of terrace heights that we observe on one level, as the same terrace can decrease in height up to ~30 meters over just a few hundred meters of horizontal distance. In the studied catchments, we find a mixture of mostly fill and strath terraces combined with a few cut terraces: The same level can be present as fill or as a bedrock strath terrace along the river. The sediment fill forming the terraces can be divided into two groups: fluvial (Ravi and Suil) and colluvium material, which are both present at all terrace levels. The fluvial material consists mostly of well- to moderately-sorted and well-rounded pebbles with grain sizes from cm to several dm, although we observed larger boulders (> 2m) in some terraces. In the Suil catchment, the pebbles are on average less rounded (Fig. 6A, B), presumably due to the shorter transport distance or less reworking. This material consists mostly of conglomerate and is the most abundant sediment across both catchments. It is mostly clast supported, but in some sections, the matrix consists of more sand and silt, which also appear as separate layers, but are less common than the conglomerate. Clay is only present in small lenses or at layer boundaries.

In contrast, the colluvium cover (Fig. 6A, B, D) is mostly moderately- to un-sorted and consists of a varying mixture of clay, silt, sand, and conglomerates, which are often mixed in a single clay or silt matrix, but there are also layers with distinct

https://doi.org/10.5194/egusphere-2026-2382
Preprint. Discussion started: 20 May 2026

grain sizes similar to the fluvial material. The conglomerate pebbles are often angular and less well-rounded than the fluvial pebbles and, in some cases, fully rectangular, although well-rounded, possibly reworked pebbles may also occur, but vary between terraces. The colluvium usually sits on the top of the fluvial terrace material as a cover layer. Its height varies from less than a meter to multiple tens of meters, and some terraces are completely covered by this material. In both the fluvial and colluvial terrace sequences, the pebbles show the same variations in lithology and indicate local sources. They mainly consist of granites, gneisses, and metasediments (slate, schist, phyllite, and quartzite). Occasionally, less metamorphosed sandstone and shale occur. The content of some lithologies varies depending on the position in the river system, e.g., more granites and gneisses start to appear at the Ravi terraces ~10 km south of Chamba near the village Mehla, where the granitic bedrock of the Dhauladhar range reaches the Ravi River (Fig. 2). In contrast, the Suil River has no granites and instead consists mostly of metasediments.

https://doi.org/10.5194/egusphere-2026-2382
Preprint. Discussion started: 20 May 2026

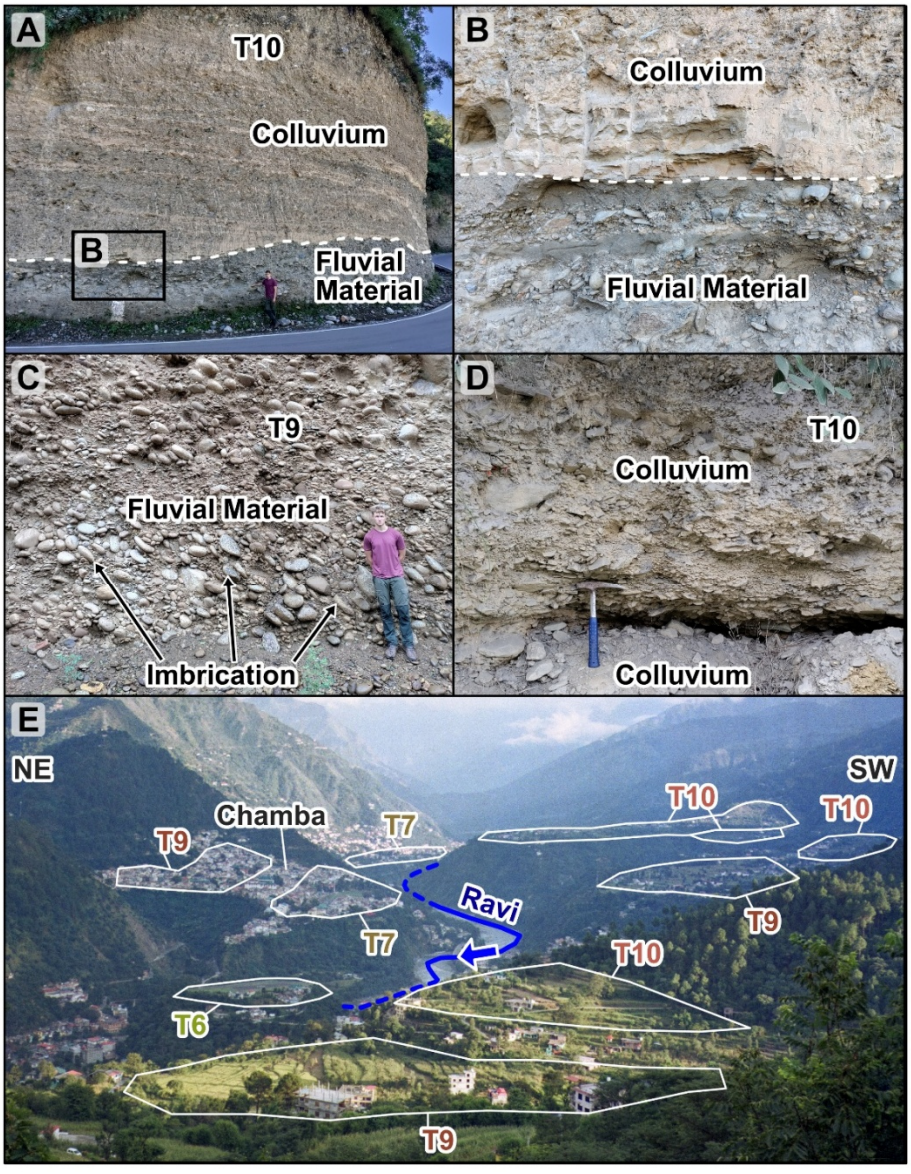

275 **Figure 6:** Field photos showing different depositional environments of terraces alongside the Suil and Ravi Rivers. The Photo locations are shown in Fig. 2. **A**: T10 terrace at the Suil River with **B** showing the marked detail section. The upper part consists of colluvium with a mixture of silt, sand, clay, and a conglomerate of well-rounded to angular pebbles. The lower part consists of a mixture of mostly well- to medium-rounded conglomerate and sand. Occasionally, a silt lens is present. The pebbles in both layers are slate, (mica) schist, phyllite, and quartzite. **C**: T9 terrace material ~1.5 km south of Chamba showing well-rounded conglomerate in a siltmatrix. Note the imbrication
280 that indicates the paleo-flow direction (towards northwest as it does today). The pebbles consist of granite, gneiss, slate, schist, and quartzite. **D**: T9 terrace level showing colluvium terrace with angular metasediment pebbles (mostly shale and slate). Please note that despite the colour change, the layer below consists of the same material, but indicates two separate deposition events. **E**: Photo of the Ravi River valley around Chamba showing exposure of various terrace levels. Height of terrace levels is shown in Fig. 3.

https://doi.org/10.5194/egusphere-2026-2382
Preprint. Discussion started: 20 May 2026

4.2 Luminescence dating

High-energy environments are likely to have greater residual and scattered OSL signals (Hu et al., 2010). However, the residuals in the present-day Ravi River sand are 2 – 4 Gy, which falls within the standard uncertainty limits of our De measurements (cf. Table 2). Thus, we did not perform residual correction to our obtained De values. Our new OSL ages (n=12) along the Ravi River yield Late Pleistocene ages, and range from 29.5 ± 2.6 ky (SD-R-02) to 12.5 ± 0.8 (SD-R5) (Table 2). The near-surface samples from the Ravi terraces yield progressively older ages with the level of the terraces. However, we also obtained smaller age variations at one terrace level along the Ravi. The lowermost sampled level (T5/T6) yields ages between 17.7 ± 1.3 ky (R-OSL-04) and 13.2 ± 0.8 (SD-18-04). For the next higher level (T7), we sampled one near-surface sample with an age of 20.5 ± 1.8 (R-OSL-05). The terrace level T9 yields the ages spanning from 29.5 ± 2.6 ky (SD-R-02) to 27.7 ± 2.2 (SD-18-02). Our two last near-surface OSL samples do not fit into the scheme of older ages with increased height above the Ravi as they yield consistent ages of 12.9 ± 0.9 ky and 12.5 ± 0.8 ky at ~300 – 350 m above the present Ravi, ~150 – 200 m higher than the T9 level (Fig. 7, Profile 3). These samples originate from a junction of the Ravi with a tributary immediately downstream of the Chamera dam and consist of angular pebbles with a higher abundance of gneiss compared to sediments transported in the Ravi. We therefore do not consider this a basin-wide Ravi terrace level but rather as an individual tributary-controlled deposit and will discuss the results separately in Supplement Text 1. Besides these two surface samples at the tributary junction, we also measured two samples from the bottom of the same sediment section right above the bedrock. There, more rounded fluvial sediment is present again at the T7 terrace level and yields the same ages as the T7 near-surface sample within error (18.6 ± 1.3 ky (SD-R2) and 18.3 ± 0.9 ky (SD-R1)). We also obtained one OSL age near the bottom of the sequence (~7 m above the present-day Ravi River), which results in an age of 16.7 ± 1.6 ky (SD-18-05). The sediment at the sampled position rises up until the height of the T9 level, with a short interruption at the T7 level. As the preserved surface of T9 is nearly twice as old, it cannot form the base of it. We therefore consider the sample as the base of T6. However, with just this one sample and the limited access to the terrace body, this classification remains speculation as indicated by question marks in Fig. 7, Profile 2.

https://doi.org/10.5194/egusphere-2026-2382
Preprint. Discussion started: 20 May 2026

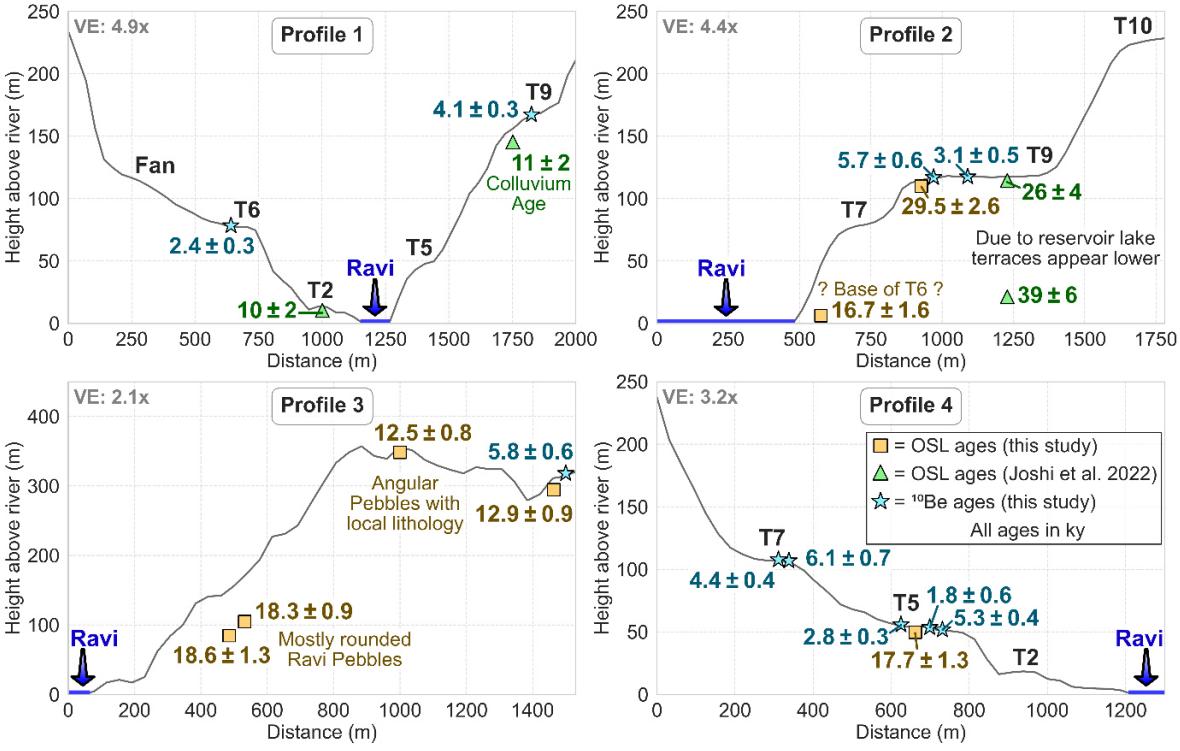

Figure 7: 4 Topographic cross profiles of the Ravi River and adjacent terraces corresponding to the profiles indicated in Fig. 3. We included all age datings of this study and the work of Joshi et al. (2022) within ~1 km distance of the profile from the same terrace levels present in the profile. All profiles are exaggerated in height. Please note that the VE, displayed in the top left, differs between each profile. Abbreviations: OSL = Optically Stimulated Luminescence, VE = Vertical Exaggeration. DEM by JAXA (AW3D30).

4.3 Cosmogenic nuclide dating

Our cosmogenic nuclide measurements yield significant and consistently younger ages compared to ages obtained by luminescence dating. For ^{10}Be, we obtained only Holocene ages, except for one sample SD17CRN12, with 16.5 ± 1.5 ky, and ages range from 10.8 ± 1.0 ky to 1.8 ± 0.6 (cf. Table 1). The ^{26}Al samples showed inconsistent results. Eight samples obtained no or a non-usable signal during measurement due to low yields in the chemical preparation, and we have discarded these ages. For 14 of our ^{26}Al samples, the measurement yielded a very low sample current compared to the standard current (< 20%), which might not be reflected in the calculated uncertainty and could result in an additional error. We therefore refrain from interpreting these ages, of which 10 also show a high uncertainty (> 25%), but we note that all 14 samples show a Holocene exposure age. The remaining 14 ^{26}Al samples show low uncertainties (max. 32%) and all except 2 samples yield identical ages to the ^{10}Be samples within uncertainty, supporting these values. We therefore decided to primarily use the ^{10}Be values for further interpretation as they yielded reliable results with low and expected analytic uncertainties.

When comparing the ^{10}Be ages with the height of the terraces, we make the following observation: The two oldest ^{10}Be ages (JK-22-36 and SD17CRN12) are obtained from the highest terraces levels preserved above the current Ravi River (~430 m and ~215 m). However, for all other samples, there is no clear correlation between terrace height and age for the Ravi (Fig.

https://doi.org/10.5194/egusphere-2026-2382
Preprint. Discussion started: 20 May 2026

8) as well as the Suil River samples (cf. Fig. 7, Profile 4). We also observe that there is no age difference if there is visible colluvium present on the terrace surface or not. Furthermore, terraces with well-rounded fluvial pebbles covering the terrace surface exhibit the same Holocene ages. Overall, no clear correlation between ^{10}Be-ages and terrace height has been recognized. These findings and observations have important implications for the interpretation of the obtained ages.

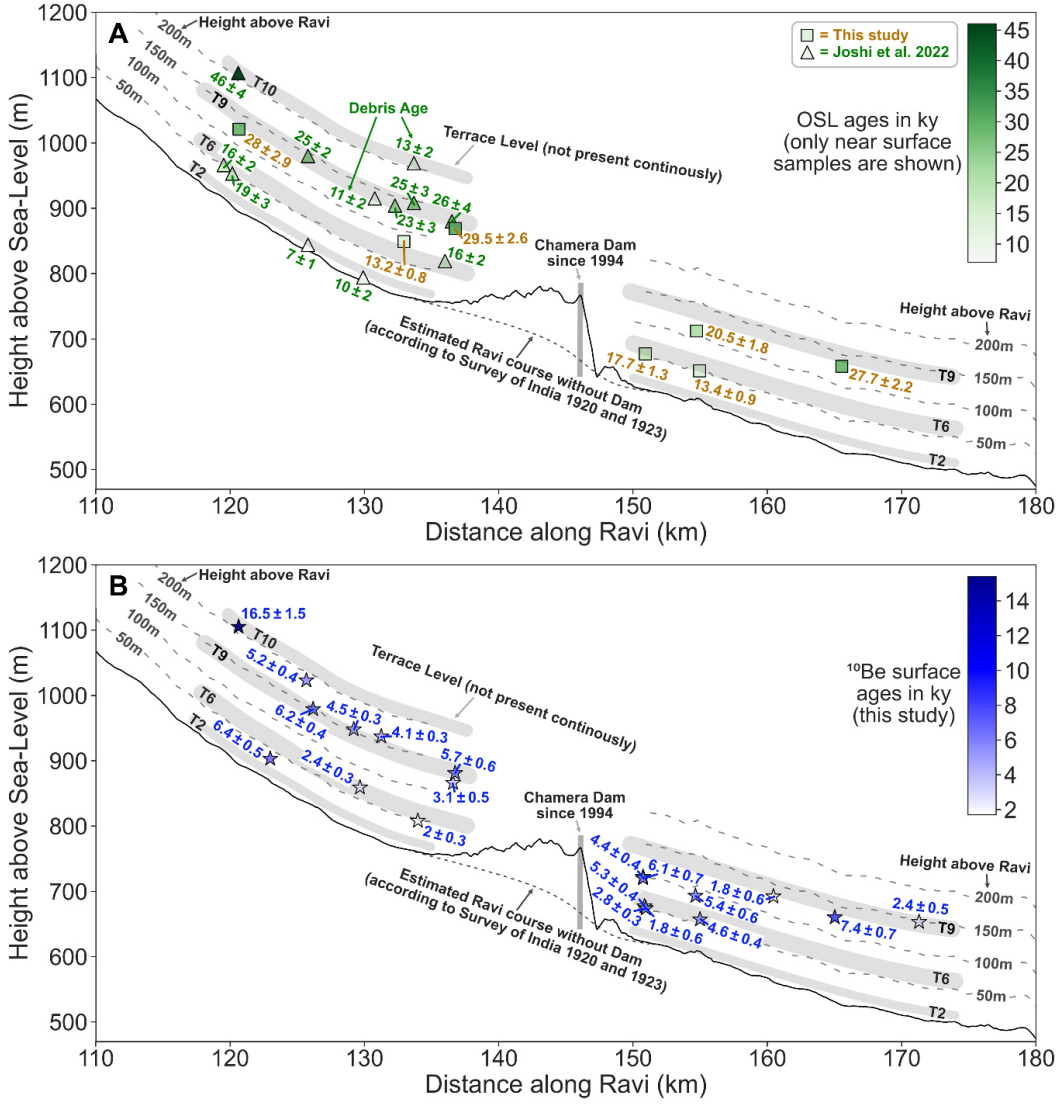

Figure 8: Topographic height profile of the Ravi River and its dominant terrace levels, including **A**: Optically stimulated luminescence (OSL) datings and **B**: Cosmogenic Nuclide (^{10}Be) ages of terraces along the Ravi. The figure only shows near-surface OSL samples that illustrate the end of deposition. All sample points have been plotted at their corresponding height at which the samples have been taken. Please note that the sketched terrace levels are not continuous and instead occur irregularly (cf. Fig. 3). OSL results of Joshi et al. (2022) are also included in A.

https://doi.org/10.5194/egusphere-2026-2382
Preprint. Discussion started: 20 May 2026

5 Discussion

5.1 Caveats of the Cosmogenic Nuclide Exposure Ages

While our OSL results align well with previously published data (Joshi et al., 2022), our cosmogenic nuclide measurements did not yield the expected ages, and the Al data have some irregularities that require further discussion. Twenty-two of the ^{26}Al measurements yielded unusable signals (n=8) or had very low sample currents during measurement (n=14), leading to potential errors. We also noted some deviation between the ^{26}Al and ^{10}Be results and investigated a potential burial signal as a cause. Six of our samples have ^{26}Al/^{10}Be ratios below 6.75, including their uncertainties, indicating transient sediment storage (e.g., Granger, 2006; Bhattacharjee et al., 2023; Mandal et al., 2023). Although these ratios resulted in burial ages up to 935 ± 573 ky (JK-22-24), we also have 4 samples with uncertainties above 6.75, which we attribute to measurement errors. We cannot rule out that a few samples experienced significant transient sediment storage, but since large ^{26}Al uncertainties affected the sample population, we cannot rely on the data to explain discrepancies between the ^{26}Al and ^{10}Be measurements. We therefore refrain from interpreting potential burial ages of these samples, but we note their presence. By relying on the ^{10}Be measurements, which universally showed low uncertainties (all except three samples below 25%), a better signal-to-noise ratio than ^{26}Al, and a good agreement with the 14 ^{26}Al samples with sufficient sample current, we make sure that our calculation of surface exposure ages is reliable and not related to potential alterations through measurement or lab errors.

However, there are two more key factors that need to be considered before surface exposure calculation and interpretation: inheritance and erosion rate. Cosmogenic nuclide accumulation before final deposition (inheritance) can result in samples appearing too old (Anderson et al., 1996). Our average of two inheritance samples results in an apparent age of 1.0 ky for both nuclides. As we do not have inheritance measurements from all terrace levels, we refrain from subtracting these values from our results. At the same time, erosion at the terrace surface can make exposure ages appear too young (Ivy-Ochs and Kober, 2008). Because we have not measured a cosmogenic depth profile, we have no reconstruction of the erosion rate at the Ravi and Suil River terrace surfaces (we could not obtain enough quartz pebbles for measurement within our 1.6 m deep pit). We therefore relied on erosion rates derived from the literature (Phillips et al., 2006; Ritz et al., 2006; Stübner et al., 2021) and used 5 mm/ky as a lower estimate (for Details see Methods 3.1). Using an estimated erosion and not accounting for inheritance may introduce unknown errors. However, our test calculations with the measured inheritance correction of two terraces and different erosion rates do not result in significantly different values (not more than 25% for n=24 samples). Because of these caveats, our cosmogenic surface exposure ages are not suitable for linking them to short-term events (< 1 ky), but instead provide the general age pattern.

When interpreting the present-day Ravi and Suil River terraces within our study area, the Chamera Dam construction from the 1990's and the associated lake need to be considered too, because it has changed the height of the terraces with respect to the river profile near the lake (cf. T9 in Fig. 8). We adjust for this by using older topographic maps (Survey of India, 1920, 1923) and showing the corrected height in our figures.

https://doi.org/10.5194/egusphere-2026-2382
Preprint. Discussion started: 20 May 2026

5.2 Sedimentation cycles of the Ravi and Suil Rivers

Our new OSL results allow us to refine the previously introduced terrace chronology of Joshi et al. (2022) in the Ravi and Suil River valleys. Starting at ~73 ky, a well-preserved terrace level aggraded to ~200 m and forms a sediment fill terrace onto the previously cut bedrock gorge in the river valley (Joshi et al., 2022). The sedimentation lasts until ~46 ky (Joshi et al., 2022), possibly with interruptions and/or temporal re-incisions. After ~46 ky, the rivers rapidly incise into the previously deposited material until the deposition of the T9 fill terrace starts at ~39 ky (Joshi et al., 2022). Our new OSL ages indicate that the sediment aggradation of this ~150 m fill terrace was completed between ~30 and 28 ky, while the previous ages of Joshi et al. (2022) suggest a slightly younger age of ~23 to 26 ky. The subsequent incision results in the formation of the ~5 – 10 m lower T8 level, which we only identified within the Suil catchment. After subsequent incision, T7 gets aggraded on top of the older material up to ~100 m above the rivers. For this level, we could not verify how deep it reaches and when the aggradation started, but the near-surface ages suggest an end of aggradation between ~21 and 18 ky. This is followed by a rapid incision that, in some segments of the rivers, removes all material of previously deposited terraces. If we interpret the SD-18-05 sample in the lower part of the deposits as the bottom of T6, the incision must have been completed by ~17 ky, but this interpretation remains speculative. The samples taken near the surface of T6 suggest a cessation of the subsequent aggradation between ~18 and ~13 ky, while the previous ages of Joshi et al. (2022) indicated an aggradation termination between ~19 and 16 ky. The deposition of T6 is followed by multiple incision events, where the lower levels T5 (~50 m height), T4 (~40 m height), and T3 (~25 m height) were carved. Joshi et al. (2022) identified the last phase of aggradation at the ~15 m high T2 level at ~10 to 7 ky, which was followed by another incision phase that marks the present-day river morphology. Widespread colluvium covering many terrace surfaces across all heights also shows post-depositional activity on many terrace surfaces. A conceptual sketch of all terrace levels, including all ages, is shown in Fig. 9. Additional observations of a terrace level below the Chamera dam, which we relate to local tributary activity, are included in the Supplement Text 1.

https://doi.org/10.5194/egusphere-2026-2382
Preprint. Discussion started: 20 May 2026

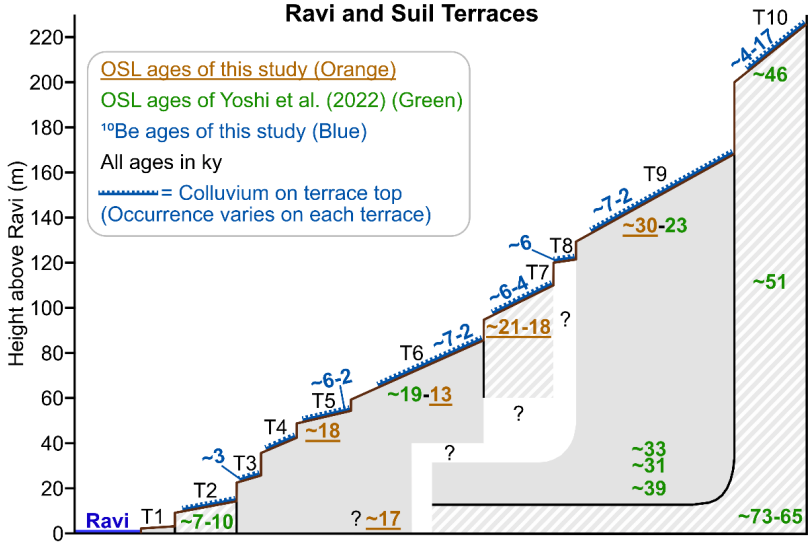

Figure 9: Sketch of the 10 terrace levels found at the investigated Ravi and Suil River sections. OSL Ages of this study and Joshi et al. (2022) are written at their sampled height within the terraces, while our ^{10}Be ages are written above the terrace. Please note that this sketch is ~6x exaggerated in height and thus terraces appear much steeper than they are (usually up to 5°), but always tilt towards the valley centre. Abbreviation: OSL = Optically Stimulated Luminescence.

5.3 Sediment transport and climate variability

Changes in the sediment transport regime of rivers can occur on seasonal to millennial timescales (e.g., Bookhagen et al., 2005; Andermann et al., 2012; Wulf et al., 2012). A key driver of these fluctuations is climate change because it controls both sediment supply and water discharge (e.g., Bookhagen et al., 2006; Dosseto et al., 2018; Dey et al., 2023). At the same time, the Himalaya tectonic activity, which usually varies on multi-millennial to million-year timescales (e.g., Dey et al., 2016a; Mandal et al., 2021; Ding et al., 2022), can lead to river blockage, path alterations, and gradient changes (e.g., Gupta, 1997; Malik et al., 2014; Wang et al., 2014). For the Ravi River, the previous study by Joshi et al. (2022) attributed the ~46 to 39 ky incision phase to a reactivation of the Chamba Trust, a proposed contact between the Higher Himalayan metasediments and the intrusions forming the peaks of the Dhauladhar Range. However, we did not find any evidence for a tectonic contact between these units and instead support the view of Fuchs and Linner (1995) that there is a continuous transition between the units with zones of contact metamorphism. While we don't rule out tectonic influences, we argue that climate changes likely play a major role in controlling the Ravi and Suil Rivers sediment regime during the late Pleistocene and Holocene. In their study, Joshi et al. (2022) found large commonalities in the aggradation and incision phases of the Ravi and other Himalayan rivers. This partly synchronous behaviour was observed in several studies of the Himalayan realm and attributed to climate variability (e.g., Ray and Srivastava, 2010; Dutta et al., 2012; Dey et al., 2016b; Sinha and Sinha, 2016; Divyadarshini et al., 2020; Singhvi et al., 2022).

To further isolate the climate response mechanisms, we focus on a comparison with Late Pleistocene and Holocene luminescence chronologies from south of the Dhauladhar Range by Srivastava et al. (2009), Thakur et al. (2014), Dey et al.

https://doi.org/10.5194/egusphere-2026-2382
Preprint. Discussion started: 20 May 2026

(2016b), and Dey et al. (2022). This is of particular interest as it offers the comparison of relatively similar source areas with important differences in glacial coverage. While there are almost no glaciers on the southern side of the Dhauladhar Range, most catchments on the northern side exhibit glacial signatures: either present-day glaciers according to the Global Land Ice Measurements from Space database (GLIMS and NSIDC, 2005 [updated 2018]) or indications of significant past glacial coverage (Fig. 1, Supplement Fig. S1). Our geomorphic landscape analysis also suggests that ~50% of the Ravi catchment was potentially influenced by glaciers in the past (Fig. 10), which is supported by previous analysis of the nearby Chenab catchment, showing a glacial extent of the main Chenab glacier down to ~2.5 km elevation (Eugster et al., 2016). We therefore expect a strong glacial influence during the Late Pleistocene north of the Dhauladhar range, in contrast to the southern range area that lacks any evidence of an extended glaciation. For the comparison with downstream areas, we focus on the past ~40 ky, because data in the northern Kangra Basin are sparse for older timeframes (Dey et al., 2022).

In the northern Kangra Basin south of the Dhauladhar range, the long term incision trend started ~42 ky ago and continued up to ~14 ky (Dey et al., 2022; Dey et al., 2016b). During this time, two short term aggradation phases have been recognized around ~31 and 20 ky (Srivastava et al., 2009; Thakur et al., 2014). During the same time window starting at ~39 ky, north of the Dhauladhar Range the aggradation of the massive T9 level starts in the Ravi and Suil River valleys (Joshi et al., 2022), which continues at least up to ~30 (this study) or 23 ky (Joshi et al., 2022). This aggradation period aligns with the end of marine isotope stage 3 (Fig. 11), where the Himalayan glaciers occupied a much larger area than in recent times (Owen et al., 2002; Ali and Juyal, 2013). During the subsequent global Last Glacial Maximum (LGM) (~24 – 18 ky) glacial reconstruction have indicated a more restricted glacial coverage, despite low temperatures, which has been linked to reduced monsoonal precipitation (Thompson et al., 1989; Owen et al., 2002; Ali and Juyal, 2013; Cheng et al., 2016; Kathayat et al., 2016). The global LGM aligns well with 2 incision periods within our study area, between ~30 (this study) or 23 (Joshi et al., 2022) to 21 ky and a second one around 18 ky (Fig. 11). The subsequent aggradation between ~18 and 13 ky within the Ravi and Suil catchments is accompanied by renewed glacial advances and an increasing monsoon strength (e.g., Ali and Juyal, 2013; Cheng et al., 2016; Kathayat et al., 2016; Saha et al., 2019), while south of the Dhauladhar range incision prevails until 14 ky (Dey et al., 2016b; Dey et al., 2022). This mostly asynchronous behaviour of sediment aggradation and incision cycles between the southern and northern Dhauladhar catchments ends in the Holocene, where the last aggradation ends at ~10 – 7 ky in both catchments (Dey et al., 2016b; Dey et al., 2022; Joshi et al., 2022). During the Holocene glaciers have further retreated (Saha et al., 2018, 2019), and their influence on aggradation in the Ravi catchment potentially decreased. The synchronicity of glacial coverage and aggradation in our study area, north of the Dhauladhar Range, is in contrast to the nearly glacier-free southern catchments. This supports the argument of Joshi et al. (2022) that glaciers were crucial in delivering material for fluvial aggradation in the Ravi catchment during the LGM.

https://doi.org/10.5194/egusphere-2026-2382
Preprint. Discussion started: 20 May 2026

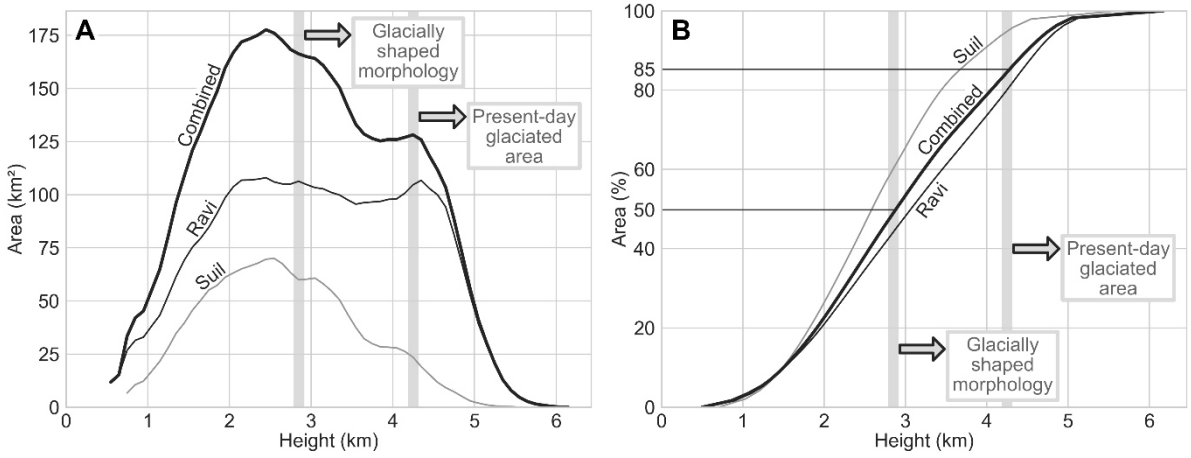

Figure 10: Hypsometric curve of the Ravi, Suil, and both catchments combined (cf. Fig. 1). Plot **A** shows the height against area, while plot **B** illustrates the height vs the cumulated area. One percentile is 100 m wide, and the Y axis area represents a 100 m wide section of the height. Vertical grey lines separate elevations with no indication of former glacial coverage (left), glacially-shaped elevations with presently no glaciers (middle), and the elevations with present-day glaciers (right). Please note that the elevation boundaries are indications and no fixed heights and may vary by a few hundred meters depending on the location.

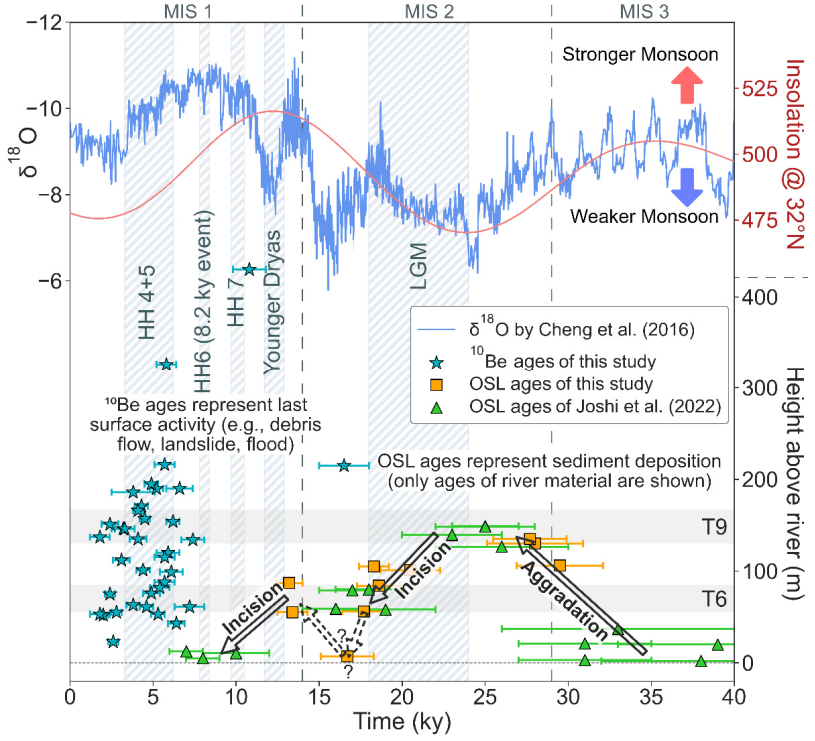

Figure 11: Cosmogenic Nuclide (^{10}Be) and optically stimulated luminescence (OSL) ages of this study and Joshi et al. (2022) plotted alongside a δ^{18}O record from Sanbao caves in China (Cheng et al., 2016), indicating changes in monsoon strength. The Marine Isotope Stages (MIS) and insolation of the study's area location are also plotted for the last 40 ky (calculator by Laskar et al. (2004). For the OSL samples, we only show the results of the river material. Arrows show long-term trends of aggradation and incision. Striped areas represent the global Last Glacial Maximum (LGM) and selected Himalayan Holocene regional glacial stages (HHs) after Saha et al. (2018).

https://doi.org/10.5194/egusphere-2026-2382
Preprint. Discussion started: 20 May 2026

Question marks indicate speculative incision/aggradation periods, because we cannot reliably assign the ~17 ky sample to a terrace level (cf. Section 4.2). Please note that glacial advances during the global LGM were limited to the Himalaya in comparison to MIS 3 (Owen et al., 2002).

5.4 Widespread Holocene overprinting of fluvial terrace surfaces across the catchment

Cosmogenic nuclide ^{10}Be surface exposure ages have been widely used as a reliable tool for dating the abandonment of fluvial terrace surfaces (e.g., Repka et al., 1997; Bookhagen et al., 2006; Rades et al., 2013). In our previous studies from the Kangra Basin south of the Dhauladhar Range, the surface exposure ages have usually been slightly but consistently younger than the luminescence ages from ~1 – 3 meters below the surface by up to a few thousand years (Dey et al., 2016b; Dey et al., 2022; Kordt et al., 2025). This is consistent with the assumption that in undisturbed sediment, the luminescence ages are representative of the last deposition during sediment aggradation, and the cosmogenic nuclide exposure age shows the timing of surface abandonment (or start of incision). However, this is not the case for the Ravi and Suil, where all terraces (except T2) yield Late Pleistocene luminescence ages but Mid- to Late Holocene ^{10}Be ages from the surface (except samples SD17CRN02 and JK-22-36). Our valid 14 ^{26}Al samples also support this chronology, with all except two samples yielding identical ages to ^{10}Be within uncertainty. We argue that the Late Pleistocene sediment deposition history is not directly linked to the formation and evolution of the present-day terrace surfaces. Because most terraces are covered with colluvial deposits, the decoupling of the OSL and ^{10}Be chronology may be expected, and they show two different geomorphic evolutionary stages: The deposition of the fluvial terrace material (OSL) and the last coverage of the terrace with colluvium (^{10}Be). However, the same Holocene ages are present for eight ^{10}Be ages, where the pebbles at the terrace surface were well-rounded, and we did not find any evidence of a colluvium cover or a different surface layer. This raises the question if there might be a significant underestimation of ^{10}Be ages in all our samples, and we discuss the possible reasons for this below.

All ages were calculated using an erosion rate of 5 mm/kyr without inheritance correction, introducing some uncertainty. But our sensitivity tests show deviations of ≤ ~50% (see Methods 3.1), which cannot explain the discrepancy, because OSL ages are consistently ~2 – 10 times older than the ^{10}Be results. An alternative explanation for young cosmogenic nuclide ages is anthropogenic disturbance, particularly agricultural ploughing, which can mix near-surface material and has been identified as a cause of age resetting in previous studies (Dey et al., 2016b; Kapannusch et al., 2020; Chauhan et al., 2026). Although many sampled terraces are cultivated, this is not universally the case, and the random distribution of ages across terrace levels argues against a systematic agricultural control (Fig. 8, 11). Previous studies from the nearby Kangra basin also showed that despite widespread agricultural use most surface exposure ages were not substantially altered (Dey et al., 2016b; Dey et al., 2016a; Kordt et al., 2025). We conclude that, although agriculture may have a minor influence, it is unlikely to be the primary cause of the observed age deviations. In the absence of analytical errors, our results instead indicate widespread Holocene reworking of nearly all Late Pleistocene terrace surfaces, regardless of the presence of colluvial cover.

We argue that there are multiple possible reasons for the Holocene terrace surface reworking and discuss them below. For the terraces that are covered with colluvium, our ^{10}Be ages most likely represent the age of deposition of the last colluvium coverage. In the High Himalaya, this is likely caused by slumps and slides in high relief landscapes (e.g., Dortch et al., 2009;

https://doi.org/10.5194/egusphere-2026-2382
Preprint. Discussion started: 20 May 2026

Dash et al., 2022). The steep mountain flanks in the Ravi and Suil valleys (mostly between ~30 and 60°) are the source areas, and present-day hillslope activity is highest during the monsoon season. Our data suggests that these mass wasting processes occur frequently at least since the Mid Holocene. Enhanced monsoonal strength during the Early-to-Mid Holocene likely has caused more landsliding due to elevated pore pressure in the upper slope layer (Pratt et al., 2002; Bookhagen et al., 2005). In addition, a permafrost retreat after the Younger Dryas could have also weakened the upper slope layer (Daanen et al., 2012; Patton et al., 2019), contributing to the observed terrace coverage.

In contrast to the terrace surfaces covered with hillslope colluvium, the geomorphological process leading to the reworking of Holocene fluvial surface deposits is less obvious. We did not observe evidence for a new depositional event, but rather argue that repeated major flooding events may have reworked the surfaces. For instance, flooding in the study area may have resulted from landslide-dammed lakes, which are common in the Himalaya (e.g., Weidinger, 1998; Sundriyal et al., 2007; Wulf et al., 2010; Ruiz-Villanueva et al., 2017). However, the absence of any preserved lacustrine deposits in our field observations suggests that any such lakes were short-lived. A more likely driver is GLOFs, triggered by the sudden release of meltwater from glacial lakes (e.g., Veh et al., 2020; Ahmed et al., 2021; Andermann et al., 2023). Given that up to ~50% of the Ravi catchment may have been influenced by glaciers during the Late Pleistocene, repeated GLOFs - particularly during post-LGM deglaciation - are expected. Modelled flood heights of up to ~70 – 80 m in Himalayan valleys (Ahmed et al., 2022; Gouli et al., 2023) suggest that lower terrace levels (up to T6) could have been directly affected, while higher sediment fills in the Late Pleistocene and Early Holocene may have enabled floods to reach higher terraces. Larger glacial extent during the Late Pleistocene potentially supported the formation of extensive lakes, increasing the magnitude and frequency of such events. Since the beginning of the Holocene, the studies by Saha et al. (2018, 2019) identified 8 regional glacial stages throughout the Himalaya. Although the extent of these glacial advances was limited after the 8.2 ky cooling event (Saha et al., 2018, 2019), the repeated fluctuations in glacial coverage potentially enhanced the likelihood of GLOFs. In addition, climate records show rapidly shifting monsoon strength since Mid-Holocene times (Srivastava et al., 2017), suggesting even faster glacial oscillations.

Beyond the immediate flood zone, GLOFs are also able to trigger widespread geomorphic changes like hillslope erosion, landslides, and rapid base-level shifts of several tens of meters (Cook et al., 2018; Chen et al., 2025; Sattar et al., 2025). GLOFs also cause seismic waves (Vuichard and Zimmermann, 1986; Iribarren Anacona et al., 2018; Feng et al., 2020), which could further promote additional mass wasting processes. Sudden high-impact events such as GLOFs could also explain the inferred base-level change at ~17 ka we attributed to the T6 terrace. Although direct sedimentary evidence of past GLOFs is limited, the presence of large, rounded boulders (>2 m in diameter) within terrace deposits and the modern riverbed indicates repeated high-magnitude flood events. The extensive glaciation of the Ravi catchment suggests that many of these were likely GLOF-related, and therefore contributing significantly to terrace modification - either directly or through secondary processes such as landsliding. In contrast, regions such as the Kangra Basin, which lack extensive glaciation and steep topography, show little evidence of comparable Holocene surface reworking (Dey et al., 2016b; Dey et al., 2016a; Dey et al., 2022).

https://doi.org/10.5194/egusphere-2026-2382
Preprint. Discussion started: 20 May 2026

Overall, we propose that a combination of frequent mass wasting, GLOFs, and steep topography led to widespread terrace reworking since at least the Mid Holocene, with climate-driven variations in monsoon intensity and glacial extent acting as key controls. We highlight that, to our knowledge, this systematic overprint of a large number of surface-exposure ages (here 36 ^{10}Be samples and 14 ^{26}Al samples) is unique and has not previously been reported from high-relief Himalayan catchments. As previous studies attributed younger cosmogenic surface ages to agriculture (e.g., Kapannusch et al., 2020; Chauhan et al., 2026), we recommend discussing other reasons for potential surface overprint in future studies, especially within the more narrow and steep river valleys within the Higher Himalaya. Given the associated hazards of the processes, further work is needed to better constrain the timing and mechanisms of surface overprinting across the Himalaya.

6 Summary

The Ravi and Suil River catchments have experienced rapid sedimentary changes during the Late Pleistocene and Holocene. Based on an updated OSL chronology with 12 new samples, 36 new ^{10}Be and 14 ^{26}Al surface exposure ages, combined with field investigations and geomorphic analysis, we make the following conclusions:

- Throughout the studied Ravi and Suil River sections, we identified 10 reoccurring terrace levels, with the four most dominant layers being T10 (~200 – 225 m), T9 (~130 – 167 m), T6 (~60 – 85 m), and T2 (~10 – 20 m) occurring mostly as strath or fill terraces, while less prominent levels have also been cut into the existing material (all heights are reported with respect to the present-day river). Most terraces feature a colluvium layer on top, with thicknesses reaching from decimeters to multiple tens of meters above the clearly different fluvial layer below. Starting from T6 level and below, many sedimentary fans of local tributaries are also present along both rivers.
- The main aggradation phases of the sampled terrace sequences were: ~73 – 46 ky (T10), ~39 – 30 or 23 ky (T9), ~21 – 18 ky (T7), ~19 – 13 ky (T6) and ~10 – 7 ky (T2) based on the compiled OSL chronology of this study and Joshi et al. (2022). We suggest that, besides monsoonal strength, glacial coverage is a key factor in contributing to aggradation/incision cycles. We have identified an extended Late Pleistocene glacial overprint in ~50% of the Ravi and Suil catchments. We argue that the influence of glaciers during cold periods is presumably larger than in nearby, almost unglaciated Himalayan catchments, where previous studies identified less aggradation during the Late Pleistocene (Dey et al., 2016b; Dey et al., 2022; Srivastava et al., 2009; Thakur et al., 2014).
- Dating the top of all terrace levels, we obtained Holocene ^{10}Be and ^{26}Al surface exposure ages, which are ~2 – 10 times younger than the near-surface OSL ages. All ages derived from ^{10}Be and ^{26}Al, except one, document Holocene surface activity, independent of a present-day colluvium cover. We suggest that, besides mass wasting processes in steep Himalayan terrain (e.g., landslides and debris flow), erosion by strong flooding events, such as Glacial Lake Outburst Floods, may have contributed to the modification of terrace surfaces and related surface exposure ages. Repeated glacial oscillations and a general decline of glacial mass within the Holocene could have favoured frequent high floods in narrow Himalayan gorges.

https://doi.org/10.5194/egusphere-2026-2382
Preprint. Discussion started: 20 May 2026

Data availability

The authors confirm that all data supporting the findings of this study are available within the article and its supplementary materials.

Author contributions

- JK: Conceptualization, Formal analysis, Investigation, Visualization, Writing (original draft preparation)
- SD: Conceptualization, Formal analysis, Writing (review and editing)
- BB: Conceptualization, Supervision, Writing (review and editing)
- GR, JL, CV: Formal analysis, Investigation, Writing (review and editing)
- NC: Formal analysis, Investigation
- RT: Conceptualization, Funding acquisition, Supervision, Writing (review and editing)

Competing interests

We declare that none of the authors has any competing interests.

Acknowledgements

This study was funded by the Deutsche Forschungsgemeinschaft (DFG) (TH 1317/8-1) and IIT Kharagpur FSRG grant to S. Dey (TIG). AMS measurements were conducted at the Ion Beam Centre (IBC) at the Helmholtz-Zentrum Dresden-Rossendorf e. V.. We would like to thank the DREAMS operator team for their assistance with AMS-measurements. We thank T. Tsering, P. Kar, and C. Singh for their assistance during fieldwork and laboratory procedures. We also thank the student M. Adam for joint fieldwork. Furthermore, we thank V. Jain (IIT Gandhinagar) for his continued support.

Financial support

This study was funded by the Deutsche Forschungsgemeinschaft (DFG) (TH 1317/8-1) and IIT Kharagpur FSRG grant to S. Dey (TIG).

https://doi.org/10.5194/egusphere-2026-2382
Preprint. Discussion started: 20 May 2026

References

Adlakha, V., Patel, R. C., Lal, N., Mehta, Y. P., Jain, A. K., and Kumar, A.: Tectonics and climate interplay: exhumation patterns of the Dhauladhar Range, Northwest Himalaya, Current Science, 104, 1551–1559, available at: http://www.jstor.org/stable/24092481, 2013.

Ahmed, R., Rawat, M., Wani, G. F., Ahmad, S. T., Ahmed, P., Jain, S. K., Meraj, G., Mir, R. A., Rather, A. F., and Farooq, M.: Glacial Lake Outburst Flood Hazard and Risk Assessment of Gangabal Lake in the Upper Jhelum Basin of Kashmir Himalaya Using Geospatial Technology and Hydrodynamic Modeling, Remote Sensing, 14, 5957, https://doi.org/10.3390/rs14235957, 2022.

Ahmed, R., Wani, G. F., Ahmad, S. T., Sahana, M., Singh, H., and Ahmed, P.: A Review of Glacial Lake Expansion and Associated Glacial Lake Outburst Floods in the Himalayan Region, Earth Syst Environ, 5, 695–708, https://doi.org/10.1007/s41748-021-00230-9, 2021.

Aitken, M. J.: An introduction to optical dating: The dating of Quaternary sediments by the use of photon-stimulated luminescence, Oxford Univ. Press, Oxford, 267 pp., 1998.

Akhmadaliev, S., Heller, R., Hanf, D., Rugel, G., and Merchel, S.: The new 6MV AMS-facility DREAMS at Dresden, Nuclear Instruments and Methods in Physics Research Section B: Beam Interactions with Materials and Atoms, 294, 5–10, https://doi.org/10.1016/j.nimb.2012.01.053, 2013.

Ali, S. N. and Juyal, N.: Chronology of Late Quaternary Glaciations in Indian Himalaya: A Critical Review, J Geol Soc India, 82, 628–638, https://doi.org/10.1007/s12594-013-0201-9, 2013.

Allen, S. K., Rastner, P., Arora, M., Huggel, C., and Stoffel, M.: Lake outburst and debris flow disaster at Kedarnath, June 2013: hydrometeorological triggering and topographic predisposition, Landslides, 13, 1479–1491, https://doi.org/10.1007/s10346-015-0584-3, 2016.

Andermann, C., Nepal, S., Wagnon, P., Veh, G., Maharjan, S. B., Azam, M. F., Brun, F., and Schwanghart, W.: Glaciers and Glacier Lake Outburst Floods in the Himalaya, in: Himalaya, Dynamics of a Giant 3, edited by: Cattin, R. and Epard, J.-L., Wiley, 55–93, https://doi.org/10.1002/9781394228683.ch3, 2023.

Andermann, C., Crave, A., Gloaguen, R., Davy, P., and Bonnet, S.: Connecting source and transport: Suspended sediments in the Nepal Himalayas, Earth and Planetary Science Letters, 351-352, 158–170, https://doi.org/10.1016/j.epsl.2012.06.059, 2012.

Anderson, R. S., Repka, J. L., and Dick, G. S.: Explicit treatment of inheritance in dating depositional surfaces using in situ 10Be and 26Al, Geol, 24, 47, https://doi.org/10.1130/0091-7613(1996)024%3C0047:ETOIID%3E2.3.CO;2, 1996.

Bailey, R. M. and Arnold, L. J.: Statistical modelling of single grain quartz De distributions and an assessment of procedures for estimating burial dose, Quaternary Science Reviews, 25, 2475–2502, https://doi.org/10.1016/j.quascirev.2005.09.012, 2006.

https://doi.org/10.5194/egusphere-2026-2382
Preprint. Discussion started: 20 May 2026

Balco, G., Stone, J. O., Lifton, N. A., and Dunai, T. J.: A complete and easily accessible means of calculating surface exposure ages or erosion rates from 10Be and 26Al measurements, Quaternary Geochronology, 3, 174–195, https://doi.org/10.1016/j.quageo.2007.12.001, 2008.

Barnard, P. L., Owen, L. A., and Finkel, R. C.: Style and timing of glacial and paraglacial sedimentation in a monsoon-influenced high Himalayan environment, the upper Bhagirathi Valley, Garhwal Himalaya, Sedimentary Geology, 165, 199–221, https://doi.org/10.1016/j.sedgeo.2003.11.009, 2004.

Benn, D. I. and Owen, L. A.: The role of the Indian summer monsoon and the mid-latitude westerlies in Himalayan glaciation: review and speculative discussion, Journal of the Geological Society, 155, 353–363, 1998.

Bhanot, V. B., Gill, J. S., Arora, R. P., and Bhalla, J. K.: Radio-metric dating of the Dalhousie granite, Current Science, 43, 208, 1974.

Bhattacharjee, S., Bookhagen, B., Sinha, R., Wieser, A., and Marchhart, O.: 26Al and 10Be concentrations from alluvial drill cores across the Indo-Gangetic plain reveal multimillion-year sediment-transport lag times, Earth and Planetary Science Letters, 619, 118318, https://doi.org/10.1016/j.epsl.2023.118318, 2023.

Blanckenburg, F. von: The control mechanisms of erosion and weathering at basin scale from cosmogenic nuclides in river sediment, Earth and Planetary Science Letters, 237, 462–479, https://doi.org/10.1016/j.epsl.2005.06.030, 2005.

Bolch, T., Kulkarni, A., Kääb, A., Huggel, C., Paul, F., Cogley, J. G., Frey, H., Kargel, J. S., Fujita, K., Scheel, M., Bajracharya, S., and Stoffel, M.: The state and fate of Himalayan glaciers, Science (New York, N.Y.), 336, 310–314, https://doi.org/10.1126/science.1215828, 2012.

Bookhagen, B., Fleitmann, D., Nishiizumi, K., Strecker, M. R., and Thiede, R. C.: Holocene monsoonal dynamics and fluvial terrace formation in the northwest Himalaya, India, Geol, 34, 601, https://doi.org/10.1130/G22698.1, 2006.

Bookhagen, B., Thiede, R. C., and Strecker, M. R.: Late Quaternary intensified monsoon phases control landscape evolution in the northwest Himalaya, Geol, 33, 149, https://doi.org/10.1130/G20982.1, 2005.

Brown, E. T., Edmond, J. M., Raisbeck, G. M., Yiou, F., Kurz, M. D., and Brook, E. J.: Examination of surface exposure ages of Antarctic moraines using in situ produced 10Be and 26Al, Geochimica et Cosmochimica Acta, 55, 2269–2283, https://doi.org/10.1016/0016-7037(91)90103-C, 1991.

Brozovic, N. and Burbank, D. W.: Dynamic fluvial systems and gravel progradation in the Himalayan foreland, Geological Society of America Bulletin, 112, 394–412, https://doi.org/10.1130/0016-7606(2000)112%3C394:DFSAGP%3E2.0.CO;2, 2000.

Chambers, J., Caddick, M., Argles, T., Horstwood, M., Sherlock, S., Harris, N., Parrish, R., and Ahmad, T.: Empirical constraints on extrusion mechanisms from the upper margin of an exhumed high-grade orogenic core, Sutlej valley, NW India, Tectonophysics, 477, 77–92, https://doi.org/10.1016/j.tecto.2008.10.013, 2009.

Chauhan, V., Mandal, S. K., Scherler, D., Panda, S. K., Das, S., and Christl, M.: Climate-driven alluvial fan aggradation and incision in an unglaciated Himalayan basin, Northwestern India, Earth Surf Processes Landf, 51, https://doi.org/10.1002/esp.70222, 2026.

https://doi.org/10.5194/egusphere-2026-2382
Preprint. Discussion started: 20 May 2026

Chen, C.-M., Hollingsworth, J., Clark, M. K., Chamlagain, D., Bista, S., Zekkos, D., Siwakoti, A., and West, A. J.: Erosional cascade during the 2021 Melamchi flood, Nature Geosci, 18, 32–36, https://doi.org/10.1038/s41561-024-01596-x, 2025.

Cheng, H., Edwards, R. L., Sinha, A., Spötl, C., Yi, L., Chen, S., Kelly, M., Kathayat, G., Wang, X., Li, X., Kong, X., Wang, Y., Ning, Y., and Zhang, H.: The Asian monsoon over the past 640,000 years and ice age terminations, Nature, 534, 640–646, https://doi.org/10.1038/nature18591, 2016.

Clift, P. D., Giosan, L., Blusztajn, J., Campbell, I. H., Allen, C., Pringle, M., Tabrez, A. R., Danish, M., Rabbani, M. M., Alizai, A., Carter, A., and Lückge, A.: Holocene erosion of the Lesser Himalaya triggered by intensified summer monsoon, Geol, 36, 79, https://doi.org/10.1130/G24315A.1, 2008.

Cook, K. L., Andermann, C., Gimbert, F., Adhikari, B. R., and Hovius, N.: Glacial lake outburst floods as drivers of fluvial erosion in the Himalaya, Science (New York, N.Y.), 362, 53–57, https://doi.org/10.1126/science.aat4981, 2018.

Daanen, R. P., Grosse, G., Darrow, M. M., Hamilton, T. D., and Jones, B. M.: Rapid movement of frozen debris-lobes: implications for permafrost degradation and slope instability in the south-central Brooks Range, Alaska, Nat. Hazards Earth Syst. Sci., 12, 1521–1537, https://doi.org/10.5194/nhess-12-1521-2012, 2012.

Dash, R. K., Falae, P. O., and Kanungo, D. P.: Debris flow susceptibility zonation using statistical models in parts of Northwest Indian Himalayas—implementation, validation, and comparative evaluation, Nat Hazards, 111, 2011–2058, https://doi.org/10.1007/s11069-021-05128-3, 2022.

Deeken, A., Thiede, R. C., Sobel, E. R., Hourigan, J. K., and Strecker, M. R.: Exhumational variability within the Himalaya of northwest India, Earth and Planetary Science Letters, 305, 103–114, https://doi.org/10.1016/j.epsl.2011.02.045, 2011.

Densmore, A. L., Sinha, R., Sinha, S., Tandon, S. K., and Jain, V.: Sediment storage and release from Himalayan piggyback basins and implications for downstream river morphology and evolution, Basin Res, 28, 446–461, https://doi.org/10.1111/bre.12116, 2016.

Dey, S., Chauhan, N., Mahala, M. K., Chakravarti, P., Vashistha, A., Jain, V., and Ray, J. S.: Dominant role of deglaciation in Late Pleistocene–Early Holocene sediment aggradation in the Upper Chenab valley, NW Himalaya, Quat. res., 113, 122–133, https://doi.org/10.1017/qua.2022.57, 2023.

Dey, S., Bookhagen, B., Thiede, R. C., Wittmann, H., Chauhan, N., Jain, V., and Strecker, M. R.: Impact of Late Pleistocene climate variability on paleo-erosion rates in the western Himalaya, Earth and Planetary Science Letters, 578, 117326, https://doi.org/10.1016/j.epsl.2021.117326, 2022.

Dey, S., Thiede, R. C., Schildgen, T. F., Wittmann, H., Bookhagen, B., Scherler, D., and Strecker, M. R.: Holocene internal shortening within the northwest Sub-Himalaya: Out-of-sequence faulting of the Jwalamukhi Thrust, India, Tectonics, 35, 2677–2697, https://doi.org/10.1002/2015TC004002, 2016a.

Dey, S., Thiede, R. C., Schildgen, T. F., Wittmann, H., Bookhagen, B., Scherler, D., Jain, V., and Strecker, M. R.: Climate-driven sediment aggradation and incision since the late Pleistocene in the NW Himalaya, India, Earth and Planetary Science Letters, 449, 321–331, https://doi.org/10.1016/j.epsl.2016.05.050, 2016b.

https://doi.org/10.5194/egusphere-2026-2382
Preprint. Discussion started: 20 May 2026

Dhiman, R. and Singh, S.: Petrogenesis and Geochemical Evolution of Dhauladhar and Dalhousie Granites, NW Himalayas, J Geol Soc India, 93, 399–408, https://doi.org/10.1007/s12594-019-1194-9, 2019.

Dimri, A. P., Thayyen, R. J., Kibler, K., Stanton, A., Jain, S. K., Tullos, D., and Singh, V. P.: A review of atmospheric and land surface processes with emphasis on flood generation in the Southern Himalayan rivers, The Science of the total environment, 556, 98–115, https://doi.org/10.1016/j.scitotenv.2016.02.206, 2016.

Ding, L., Kapp, P., Cai, F., Garzione, C. N., Xiong, Z., Wang, H., and Wang, C.: Timing and mechanisms of Tibetan Plateau uplift, Nat Rev Earth Environ, 3, 652–667, https://doi.org/10.1038/s43017-022-00318-4, 2022.

Divyadarshini, A., Singh, V., Jaiswal, M. K., and Rawat, M.: Exploring the roles of climate and tectonics in the geomorphic evolution of the Chitwan Intermontane valley, Central Himalaya, Geomorphology, 367, 107298, https://doi.org/10.1016/j.geomorph.2020.107298, 2020.

Dortch, J. M., Owen, L. A., Haneberg, W. C., Caffee, M. W., Dietsch, C., and Kamp, U.: Nature and timing of large landslides in the Himalaya and Transhimalaya of northern India, Quaternary Science Reviews, 28, 1037–1054, https://doi.org/10.1016/j.quascirev.2008.05.002, 2009.

Dosseto, A., May, J.-H., Choi, J.-H., Swander, Z. J., Fink, D., Korup, O., Hesse, P., Singh, T., Mifsud, C., and Srivastava, P.: Late quaternary fluvial incision and aggradation in the Lesser Himalaya, India, Quaternary Science Reviews, 197, 112–128, https://doi.org/10.1016/j.quascirev.2018.07.035, 2018.

Dubey, S., Sattar, A., Goyal, M. K., Allen, S., Frey, H., Haritashya, U. K., and Huggel, C.: Mass Movement Hazard and Exposure in the Himalaya, Earth's Future, 11, https://doi.org/10.1029/2022EF003253, 2023.

Durcan, J. A., King, G. E., and Duller, G. A.: DRAC: Dose Rate and Age Calculator for trapped charge dating, Quaternary Geochronology, 28, 54–61, https://doi.org/10.1016/j.quageo.2015.03.012, 2015.

Dutta, S., Suresh, N., and Kumar, R.: Climatically controlled Late Quaternary terrace staircase development in the fold- and -thrust belt of the Sub Himalaya, Palaeogeography, Palaeoclimatology, Palaeoecology, 356-357, 16–26, https://doi.org/10.1016/j.palaeo.2011.05.006, 2012.

Eugster, P., Scherler, D., Thiede, R. C., Codilean, A. T., and Strecker, M. R.: Rapid Last Glacial Maximum deglaciation in the Indian Himalaya coeval with midlatitude glaciers: New insights from 10 Be-dating of ice-polished bedrock surfaces in the Chandra Valley, NW Himalaya, Geophys. Res. Lett., 43, 1589–1597, https://doi.org/10.1002/2015GL066077, 2016.

Feng, Z.-Y., Huang, H.-Y., and Chen, S.-C.: Analysis of the characteristics of seismic and acoustic signals produced by a dam failure and slope erosion test, Landslides, 17, 1605–1618, https://doi.org/10.1007/s10346-020-01390-x, 2020.

Fuchs, G.: Contributions to the geology of the north-western Himalayas, Abhandlungen der geologischen Bundesanstalt, 1–59, 1975.

Fuchs, G. and Linner, M.: Geological traverse across the western Himalaya—a contribution to the geology of eastern Ladakh, Lahul, and Chamba, Jahrbuch der Geologischen Bundesanstalt, 138, 665–685, 1995.

https://doi.org/10.5194/egusphere-2026-2382
Preprint. Discussion started: 20 May 2026

Funk, C. C., Peterson, P. J., Landsfeld, M. F., Pedreros, D. H., Verdin, J. P., Rowland, J. D., Romero, B. E., Husak, G. J., Michaelsen, J. C., and Verdin, A. P.: A quasi-global precipitation time series for drought monitoring, US Geological Survey, 2014.

Gansser, A.: The geodynamic history of the Himalaya, in: Zagros, Hindu Kush, Himalaya: Geodynamic Evolution, edited by: Gupta, H. K. and Delany, F. M., American Geophysical Union, Washington, D. C., 111–121, https://doi.org/10.1029/gd003p0111, 1981.

Gavillot, Y., Meigs, A. J., Sousa, F. J., Stockli, D., Yule, D., and Malik, M.: Late Cenozoic Foreland-to-Hinterland Low-Temperature Exhumation History of the Kashmir Himalaya, Tectonics, 37, 3041–3068, https://doi.org/10.1029/2017TC004668, 2018.

GLIMS and NSIDC: GLIMS Glacier Database, Version 1: Global Land Ice Measurements from Space glacier database. Compiled and made available by the international GLIMS community and the National Snow and Ice Data Center, Boulder CO, U.S.A., 2005 (updated 2018).

Gouli, M. R., Hu, K., Khadka, N., and Talchabhadel, R.: Hazard assessment of a pair of glacial lakes in Nepal Himalaya: unfolding combined outbursts of Upper and Lower Barun, Geomatics, Natural Hazards and Risk, 14, https://doi.org/10.1080/19475705.2023.2266219, 2023.

Granger, D. E.: A review of burial dating methods using 26Al and 10Be, in: In Situ-Produced Cosmogenic Nuclides and Quantification of Geological Processes, edited by: Alonso-Zarza, A. M. and Tanner, L. H., Geological Society of America, https://doi.org/10.1130/2006.2415(01), 2006.

Gupta, S.: Himalayan drainage patterns and the origin of fluvial megafans in the Ganges foreland basin, Geol, 25, 11, https://doi.org/10.1130/0091-7613(1997)025%3C0011:HDPATO%3E2.3.CO;2, 1997.

Hu, G., Zhang, J.-F., Qiu, W.-L., and Zhou, L.-P.: Residual OSL signals in modern fluvial sediments from the Yellow River (HuangHe) and the implications for dating young sediments, Quaternary Geochronology, 5, 187–193, https://doi.org/10.1016/j.quageo.2009.05.003, 2010.

Iribarren Anacona, P., Norton, K., Mackintosh, A., Escobar, F., Allen, S., Mazzorana, B., and Schaefer, M.: Dynamics of an outburst flood originating from a small and high-altitude glacier in the Arid Andes of Chile, Nat Hazards, 94, 93–119, https://doi.org/10.1007/s11069-018-3376-y, 2018.

Ivy-Ochs, S. and Kober, F.: Surface exposure dating with cosmogenic nuclides, E&G Quaternary Sci. J., 57, 179–209, https://doi.org/10.3285/eg.57.1-2.7, 2008.

Jaegaer, E.: Rb-Sr age determinations on biotites and whole rock samples from Mandi and Chor Granites, Himachal Pradesh, India, Ecol. Geol. Helv., 64, 521–527, 1971.

Joshi, M., Thakur, V. C., Suresh, N., and Sundriyal, Y. P.: Climate-tectonic imprints on the Late Quaternary Ravi River Valley Terraces of the Chamba region in the NW Himalaya, Journal of Asian Earth Sciences, 223, 104990, https://doi.org/10.1016/j.jseaes.2021.104990, 2022.

Julien, P. Y.: Erosion and Sedimentation, Cambridge University Press, 2012.

https://doi.org/10.5194/egusphere-2026-2382
Preprint. Discussion started: 20 May 2026

Kapannusch, R., Scherler, D., King, G., and Wittmann, H.: Glacial influence on late Pleistocene 10Be-derived paleo-erosion rates in the north-western Himalaya, India, Earth and Planetary Science Letters, 547, 116441, https://doi.org/10.1016/j.epsl.2020.116441, 2020.

Kathayat, G., Cheng, H., Sinha, A., Spötl, C., Edwards, R. L., Zhang, H., Li, X., Yi, L., Ning, Y., Cai, Y., Lui, W. L., and Breitenbach, S. F. M.: Indian monsoon variability on millennial-orbital timescales, Scientific reports, 6, 24374, https://doi.org/10.1038/srep24374, 2016.

Kirby, E. and Whipple, K.: Quantifying differential rock-uplift rates via stream profile analysis, Geol, 29, 415, https://doi.org/10.1130/0091-7613(2001)029<0415:QDRURV>2.0.CO;2, 2001.

Kohl, C. and Nishiizumi, K.: Chemical isolation of quartz for measurement of in-situ-produced cosmogenic nuclides, Geochimica et Cosmochimica Acta, 56, 3583–3587, https://doi.org/10.1016/0016-7037(92)90401-4, 1992.

Kordt, J., Dey, S., Bookhagen, B., Rugel, G., Lachner, J., Vivo-Vilches, C., Panda, S. K., Chauhan, N., and Thiede, R.: Rapid Late Pleistocene Frontal Fault Growth and Sutlej Drainage Reorganization in the Western Himalaya, Lithosphere, 2025, https://doi.org/10.2113/2025/lithosphere_2025_127, 2025.

Lachner, J., Rugel, G., Vivo Vilches, C., Koll, D., Stübner, K., Winkler, S., and Wallner, A.: Optimization of 10Be measurements at the 6 MV AMS facility DREAMS, Nuclear Instruments and Methods in Physics Research Section B: Beam Interactions with Materials and Atoms, 535, 29–33, https://doi.org/10.1016/j.nimb.2022.11.008, 2023.

Lapp, T., Kook, M., Murray, A. S., Thomsen, K. J., Buylaert, J.-P., and Jain, M.: A new luminescence detection and stimulation head for the Risø TL/OSL reader, Radiation Measurements, 81, 178–184, https://doi.org/10.1016/j.radmeas.2015.02.001, 2015.

Laskar, J., Robutel, P., Joutel, F., Gastineau, M., Correia, A. C. M., and Levrard, B.: A long-term numerical solution for the insolation quantities of the Earth, A&A, 428, 261–285, https://doi.org/10.1051/0004-6361:20041335, 2004.

Le Fort, P.: Himalayas: the collided range. Present knowledge of the continental arc, American Journal of Science, 275, 1–44, 1975.

Lifton, N., Sato, T., and Dunai, T. J.: Scaling in situ cosmogenic nuclide production rates using analytical approximations to atmospheric cosmic-ray fluxes, Earth and Planetary Science Letters, 386, 149–160, https://doi.org/10.1016/j.epsl.2013.10.052, 2014.

Malik, J. N., Shah, A. A., Naik, S. P., Sahoo, S., Okumura, K., and Patra, N. R.: Active fault study along foothill zone of Kumaun Sub-Himalaya: influence on landscape shaping and drainage evolution, Current Science, 106, 229–236, available at: http://www.jstor.org/stable/24099803, 2014.

Mandal, S. K., Kapannusch, R., Scherler, D., Barnes, J. B., Insel, N., and Densmore, A. L.: Cosmogenic Nuclide Tracking of Sediment Recycling From a Frontal Siwalik Range in the Northwestern Himalaya, J. Geophys. Res. Earth Surf., 128, https://doi.org/10.1029/2023JF007164, 2023.

Mandal, S. K., Scherler, D., and Wittmann, H.: Tectonic Accretion Controls Erosional Cyclicity in the Himalaya, AGU Advances, 2, https://doi.org/10.1029/2021AV000487, 2021.

https://doi.org/10.5194/egusphere-2026-2382
Preprint. Discussion started: 20 May 2026

Montgomery, D. R. and Buffington, J. M.: Channel-reach morphology in mountain drainage basins, Geological Society of America Bulletin, 109, 596–611, https://doi.org/10.1130/0016-7606(1997)109%3C0596:CRMIMD%3E2.3.CO;2, 1997.

Murray, A. S. and Wintle, A. G.: The single aliquot regenerative dose protocol: potential for improvements in reliability, Radiation Measurements, 37, 377–381, https://doi.org/10.1016/S1350-4487(03)00053-2, 2003.

Najman, Y., Johnson, K., White, N., and Oliver, G.: Evolution of the Himalayan foreland basin, NW India, Basin Res, 16, 1–24, https://doi.org/10.1111/j.1365-2117.2004.00223.x, 2004.

Ouchi, S.: Response of alluvial rivers to slow active tectonic movement, Geological Society of America Bulletin, 96, 504, https://doi.org/10.1130/0016-7606(1985)96%3C504:ROARTS%3E2.0.CO;2, 1985.

Owen, L. A. and Dortch, J. M.: Nature and timing of Quaternary glaciation in the Himalayan–Tibetan orogen, Quaternary Science Reviews, 88, 14–54, https://doi.org/10.1016/j.quascirev.2013.11.016, 2014.

Owen, L. A., Finkel, R. C., and Caffee, M. W.: A note on the extent of glaciation throughout the Himalaya during the global Last Glacial Maximum, Quaternary Science Reviews, 21, 147–157, https://doi.org/10.1016/S0277-3791(01)00104-4, 2002.

Parida, S., Kaushal, R. K., Chauhan, N., and Singhvi, A. K.: Changes in thermoluminescence sensitivity of 110°C glow peak of quartz grains from sediments of River Ganga: Observation and implications, Earth and Planetary Science Letters, 656, 119267, https://doi.org/10.1016/j.epsl.2025.119267, 2025.

Patton, A. I., Rathburn, S. L., and Capps, D. M.: Landslide response to climate change in permafrost regions, Geomorphology, 340, 116–128, https://doi.org/10.1016/j.geomorph.2019.04.029, 2019.

Phillips, W. M., Hall, A. M., Mottram, R., Fifield, L. K., and Sugden, D. E.: Cosmogenic 10Be and 26Al exposure ages of tors and erratics, Cairngorm Mountains, Scotland: Timescales for the development of a classic landscape of selective linear glacial erosion, Geomorphology, 73, 222–245, https://doi.org/10.1016/j.geomorph.2005.06.009, 2006.

Pratt, B., Burbank, D. W., Heimsath, A., and Ojha, T.: Impulsive alluviation during early Holocene strengthened monsoons, central Nepal Himalaya, Geol, 30, 911, https://doi.org/10.1130/0091-7613(2002)030%3C0911:IADEHS%3E2.0.CO;2, 2002.

Rades, E. F., Hetzel, R., Xu, Q., and Ding, L.: Constraining Holocene lake-level highstands on the Tibetan Plateau by 10Be exposure dating: a case study at Tangra Yumco, southern Tibet, Quaternary Science Reviews, 82, 68–77, https://doi.org/10.1016/j.quascirev.2013.09.016, 2013.

Ray, Y. and Srivastava, P.: Widespread aggradation in the mountainous catchment of the Alaknanda–Ganga River System: timescales and implications to Hinterland–foreland relationships, Quaternary Science Reviews, 29, 2238–2260, https://doi.org/10.1016/j.quascirev.2010.05.023, 2010.

Repka, J. L., Anderson, R. S., and Finkel, R. C.: Cosmogenic dating of fluvial terraces, Fremont River, Utah, Earth and Planetary Science Letters, 152, 59–73, https://doi.org/10.1016/S0012-821X(97)00149-0, 1997.

Ritz, J., Vassallo, R., Brakcher, R., Brown, E. T., Carretier, S., and Bourlès, D. L.: Using in situ-produced 10Be to quantify active tectomics in the Gurvan Bogd mountain range (Gobi-Altay, Mongolia), Special Papers-Geological Society of America, 415, 87, 2006.

https://doi.org/10.5194/egusphere-2026-2382
Preprint. Discussion started: 20 May 2026

Roberts, H. M.: Assessing the effectiveness of the double-SAR protocol in isolating a luminescence signal dominated by quartz, Radiation Measurements, 42, 1627–1636, https://doi.org/10.1016/j.radmeas.2007.09.010, 2007.

Rugel, G., Pavetich, S., Akhmadaliev, S., Enamorado Baez, S. M., Scharf, A., Ziegenrücker, R., and Merchel, S.: The first four years of the AMS-facility DREAMS: Status and developments for more accurate radionuclide data, Nuclear Instruments and Methods in Physics Research Section B: Beam Interactions with Materials and Atoms, 370, 94–100, https://doi.org/10.1016/j.nimb.2016.01.012, 2016.

Ruiz-Villanueva, V., Allen, S., Arora, M., Goel, N. K., and Stoffel, M.: Recent catastrophic landslide lake outburst floods in the Himalayan mountain range, Progress in Physical Geography: Earth and Environment, 41, 3–28, https://doi.org/10.1177/0309133316658614, 2017.

Saha, S., Owen, L. A., Orr, E. N., and Caffee, M. W.: High-frequency Holocene glacier fluctuations in the Himalayan-Tibetan orogen, Quaternary Science Reviews, 220, 372–400, https://doi.org/10.1016/j.quascirev.2019.07.021, 2019.

Saha, S., Owen, L. A., Orr, E. N., and Caffee, M. W.: Timing and nature of Holocene glacier advances at the northwestern end of the Himalayan-Tibetan orogen, Quaternary Science Reviews, 187, 177–202, https://doi.org/10.1016/j.quascirev.2018.03.009, 2018.

Sattar, A., Cook, K. L., Rai, S. K., Berthier, E., Allen, S., Rinzin, S., van Vries, M. W. de, Haeberli, W., Kushwaha, P., Shugar, D. H., Emmer, A., Haritashya, U. K., Frey, H., Rao, P., Gurudin, K. S. K., Rai, P., Rajak, R., Hossain, F., Huggel, C., Mergili, M., Azam, M. F., Gascoin, S., Carrivick, J. L., Bell, L. E., Ranjan, R. K., Rashid, I., Kulkarni, A. V., Petley, D., Schwanghart, W., Watson, C. S., Islam, N., Gupta, M. D., Lane, S. N., and Bhat, S. Y.: The Sikkim flood of October 2023: Drivers, causes, and impacts of a multihazard cascade, Science (New York, N.Y.), 387, eads2659, https://doi.org/10.1126/science.ads2659, 2025.

Scherler, D., Bookhagen, B., Wulf, H., Preusser, F., and Strecker, M. R.: Increased late Pleistocene erosion rates during fluvial aggradation in the Garhwal Himalaya, northern India, Earth and Planetary Science Letters, 428, 255–266, https://doi.org/10.1016/j.epsl.2015.06.034, 2015.

Schumm, S. A.: The fluvial system, A Wiley-Interscience publication, Wiley, New York, 338 pp., 1977.

Seeber, L. and Gornitz, V.: River profiles along the Himalayan arc as indicators of active tectonics, Tectonophysics, 92, 335–367, https://doi.org/10.1016/0040-1951(83)90201-9, 1983.

Sharma, B. K. and Bhola, A. M.: Kink bands in the Chamba region, Western Himalaya, India, Journal of Asian Earth Sciences, 25, 513–528, https://doi.org/10.1016/j.jseaes.2004.05.003, 2005.

Shroder, J. F. and Bishop, M. P.: Mass movement in the Himalaya: new insights and research directions, Geomorphology, 26, 13–35, https://doi.org/10.1016/S0169-555X(98)00049-X, 1998.

Simon, A. and Rinaldi, M.: Disturbance, stream incision, and channel evolution: The roles of excess transport capacity and boundary materials in controlling channel response, Geomorphology, 79, 361–383, https://doi.org/10.1016/j.geomorph.2006.06.037, 2006.

https://doi.org/10.5194/egusphere-2026-2382
Preprint. Discussion started: 20 May 2026

Singhvi, A. K., Kaushal, R. K., and Parida, S.: Luminescence dating and Quaternary Geology: The Indian Narrative, Journal of the Palaeontological Society of India, 67, 183–210, https://doi.org/10.1177/0971102320220114, 2022.

Sinha, S. and Sinha, R.: Geomorphic evolution of Dehra Dun, NW Himalaya: Tectonics and climatic coupling, Geomorphology, 266, 20–32, https://doi.org/10.1016/j.geomorph.2016.05.002, 2016.

Srivastava, P., Rajak, M. K., and Singh, L. P.: Late Quaternary alluvial fans and paleosols of the Kangra basin, NW Himalaya: Tectonic and paleoclimatic implications, CATENA, 76, 135–154, https://doi.org/10.1016/j.catena.2008.10.004, 2009.

Srivastava, P., Agnihotri, R., Sharma, D., Meena, N., Sundriyal, Y. P., Saxena, A., Bhushan, R., Sawlani, R., Banerji, U. S., Sharma, C., Bisht, P., Rana, N., and Jayangondaperumal, R.: 8000-year monsoonal record from Himalaya revealing reinforcement of tropical and global climate systems since mid-Holocene, Scientific reports, 7, 14515, https://doi.org/10.1038/s41598-017-15143-9, 2017.

Steck, A.: Geology of the NW Indian Himalaya, Eclogae Geologicae Helvetiae, 96, 147–196, 2003.

Stübner, K., Bookhagen, B., Merchel, S., Lachner, J., and Gadoev, M.: Unravelling the Pleistocene glacial history of the Pamir mountains, Central Asia, Quaternary Science Reviews, 257, 106857, https://doi.org/10.1016/j.quascirev.2021.106857, 2021.

Sundriyal, Y. P., Tripathi, J. K., Sati, S. P., Rawat, G. S., and Srivastava, P.: Landslide-dammed lakes in the Alaknanda Basin, Lesser Himalaya: Causes and implications, Current Science (00113891), 93, 2007.

Survey of India: Punjab & Punjab States: Gurdaspur District and Chamba State, Survey of India, Calcutta, No. 52D, Sheet 2, 1923.

Survey of India: Kashmir & Jammu & Punjab: Kathua & Gurdaspur Districts & Chamba State, Survey of India, Calcutta, No. 43P, Sheet 14, 1920.

Thakur, V. C.: Structure of the Chamba nappe and position of the Main Central Thrust in Kashmir Himalaya, Journal of Asian Earth Sciences, 16, 269–282, https://doi.org/10.1016/S0743-9547(98)00011-7, 1998.

Thakur, V. C.: Geology of Western Himalaya, 19, Pergamon Press, Oxford, 1 pp., 1992.

Thakur, V. C., Joshi, M., Sahoo, D., Suresh, N., Jayangondapermal, R., and Singh, A.: Partitioning of convergence in Northwest Sub-Himalaya: estimation of late Quaternary uplift and convergence rates across the Kangra reentrant, North India, Int J Earth Sci (Geol Rundsch), 103, 1037–1056, https://doi.org/10.1007/s00531-014-1016-7, 2014.

Thiede, R., Robert, X., Stübner, K., Dey, S., and Faruhn, J.: Sustained out-of-sequence shortening along a tectonically active segment of the Main Boundary thrust: The Dhauladhar Range in the northwestern Himalaya, Lithosphere, 9, 715–725, https://doi.org/10.1130/L630.1, 2017.

Thompson, L. G., Mosley-Thompson, E., Davis, M. E., Bolzan, J. F., Dai, J., Klein, L., Yao, T., Wu, X., Xie, Z., and Gundestrup, N.: Holocene—late pleistocene climatic ice core records from qinghai-tibetan plateau, Science (New York, N.Y.), 246, 474–477, https://doi.org/10.1126/science.246.4929.474, 1989.

https://doi.org/10.5194/egusphere-2026-2382
Preprint. Discussion started: 20 May 2026

Tofelde, S., Bufe, A., and Turowski, J. M.: Hillslope Sediment Supply Limits Alluvial Valley Width, AGU Advances, 3, https://doi.org/10.1029/2021AV000641, 2022.

Veh, G., Korup, O., and Walz, A.: Hazard from Himalayan glacier lake outburst floods, Proceedings of the National Academy of Sciences of the United States of America, 117, 907–912, https://doi.org/10.1073/pnas.1914898117, 2020.

Vuichard, D. and Zimmermann, M.: The Langmoche Flash-Flood, Khumbu Himal, Nepal, Mountain Research and Development, 6, 90, https://doi.org/10.2307/3673345, 1986.

Wang, P., Chen, J., Dai, F., Long, W., Xu, C., Sun, J., and Cui, Z.: Chronology of relict lake deposits around the Suwalong paleolandslide in the upper Jinsha River, SE Tibetan Plateau: Implications to Holocene tectonic perturbations, Geomorphology, 217, 193–203, https://doi.org/10.1016/j.geomorph.2014.04.027, 2014.

Watanbe, T. and Rothacher, D.: The 1994 Lugge Tsho Glacial Lake Outburst Flood, Bhutan Himalaya, Mountain Research and Development, 16, 77, https://doi.org/10.2307/3673897, 1996.

Weidinger, J. T.: Case history and hazard analysis of two lake-damming landslides in the Himalayas, Journal of Asian Earth Sciences, 16, 323–331, https://doi.org/10.1016/S0743-9547(98)00026-9, 1998.

White, N. M., Pringle, M., Garzanti, E., Bickle, M., Najman, Y., Chapman, H., and Friend, P.: Constraints on the exhumation and erosion of the High Himalayan Slab, NW India, from foreland basin deposits, Earth and Planetary Science Letters, 195, 29–44, https://doi.org/10.1016/S0012-821X(01)00565-9, 2002.

Wulf, H., Bookhagen, B., and Scherler, D.: Climatic and geologic controls on suspended sediment flux in the Sutlej River Valley, western Himalaya, Hydrol. Earth Syst. Sci., 16, 2193–2217, https://doi.org/10.5194/hess-16-2193-2012, 2012.

Wulf, H., Bookhagen, B., and Scherler, D.: Seasonal precipitation gradients and their impact on fluvial sediment flux in the Northwest Himalaya, Geomorphology, 118, 13–21, https://doi.org/10.1016/j.geomorph.2009.12.003, 2010.